

A Simple Oscillator Using Memristor

**Maheshwar Pd. Sah, Vetriveeran Rajamani, Zubaer Ibna Mannan,
Abdullah Eroglu, Hyongsuk Kim and Leon Chua**

Abstract This paper presents a simple oscillator using a battery and a second order memristor without the energy storage elements inductor and capacitor. The oscillating mechanism of the proposed circuit has been explained via Hopf bifurcation theorem, small signal model, local activity principle and edge of chaos theorem. This paper can be also used as a reference for explaining the intimate relationship between the super-critical *Hopf bifurcation phenomenon* and the *edge of chaos*.

Keywords Memristor • Pinched hysteresis loop • Oscillator • Local activity • Edge of chaos • Super-critical Hopf-bifurcation

M.Pd. Sah • A. Eroglu

School of Applied Sciences and Engineering Technology, Ivy Tech Community College,
Evansville, IN 47710, USA
e-mail: sahmaheshwar@gmail.com

A. Eroglu

e-mail: eroglua@ipfw.edu

M.Pd. Sah

Department of Electrical and Computer Engineering, Purdue University Fort Wayne,
Fortwayne, IN 46805, USA

M.Pd.Sah • V. Rajamani • Z.I. Mannan • H. Kim (✉)

Division of Electronics and Information Engineering, Chonbuk National University,
Jeonju, Jeonbuk 54896, South Korea
e-mail: hskim@jbnu.ac.kr

V. Rajamani

e-mail: vetrieece86@gmail.com

Z.I. Mannan

e-mail: zimannan@gmail.com

L. Chua

Department of Electrical Engineering and Computer Sciences, University of California,
Berkeley, CA 94720, USA
e-mail: chua@berkeley.edu

L. Chua

TUM Fakultät für Elektrotechnik und Informationstechnik, Technische Universität München,
Arcisstrasse 21, Munich 80333, Germany

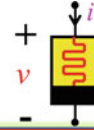
1 Introduction

An electronic oscillator circuit is generally designed by using one linear capacitor and one linear inductor, or two linear capacitors, or two linear inductors, along with a locally-active nonlinear 2-terminal resistor having a negative slope region in the DC V - I curve (e.g., a tunnel diode), or a locally-passive nonlinear 2-terminal resistor (e.g., p-n junction diode, zener diode, varistor, etc.), and a locally-active 3-terminal resistor, such as a transistor, in addition to the ubiquitous battery, required to satisfy the *first law of thermodynamics*. Examples of tunnel diode oscillator (Mehta and Mehta 2005) and the well-known Wien-bridge oscillator¹ are shown in Fig. 1a and b respectively.

Figure 1c represents the world's simplest electronic oscillator containing *only one memristor* connected in parallel with a battery.

The *memristor* in this circuit is a generic (Chua 2014, 2015; Mannan et al. 2016; Rajamani et al. 2016) *2nd-order locally-active memristor* described by the following state-dependent Ohm's law and state equations:

Second-Order Memristor



State-Dependent Ohm's Law:

$$i = G(x_1, x_2) v \quad 1(a)$$

where

$$G(x_1, x_2) = \frac{1}{\left(K_1 e^{\beta_1(x_1 - \gamma_1)} \right) + \left(K_2 e^{\beta_2 \left(\frac{1}{x_2} - \frac{1}{\gamma_2} \right)} \right)} \quad 1(b)$$

State Equations:

$$\frac{dx_1}{dt} = \frac{1}{\alpha_1} \left[\delta_1 (\gamma_1 - x_1) + \frac{K_1 e^{\beta_1(x_1 - \gamma_1)}}{\left(\left(K_1 e^{\beta_1(x_1 - \gamma_1)} \right) + \left(K_2 e^{\beta_2 \left(\frac{1}{x_2} - \frac{1}{\gamma_2} \right)} \right) \right)^2} v^2 \right] \triangleq f_1(x_1, x_2, v) \quad 1(c)$$

$$\frac{dx_2}{dt} = \frac{1}{\alpha_2} \left[\delta_2 (\gamma_2 - x_2) + \frac{K_2 e^{\beta_2 \left(\frac{1}{x_2} - \frac{1}{\gamma_2} \right)}}{\left(\left(K_1 e^{\beta_1(x_1 - \gamma_1)} \right) + \left(K_2 e^{\beta_2 \left(\frac{1}{x_2} - \frac{1}{\gamma_2} \right)} \right) \right)^2} v^2 \right] \triangleq f_2(x_1, x_2, v) \quad 1(d)$$

¹The circuit diagram of the Wien-bridge oscillator can be found from the following link <http://www.circuitstoday.com/wien-bridge-oscillator>.

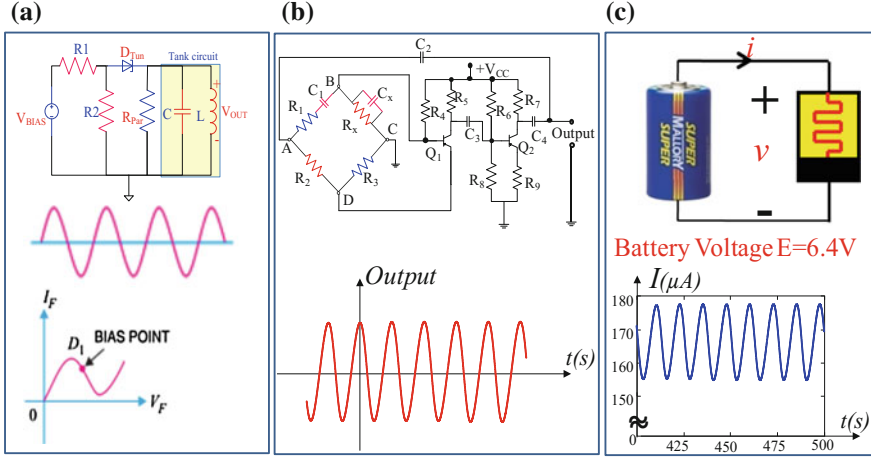


Fig. 1 **a** Simplest oscillator using a tunnel diode and an LC tank circuit (Mehta 2005). **b** Wien-bridge oscillator using resistors, capacitors and transistors (see footnote 1). **c** World's simplest oscillator using only one memristor. The blue near-sinusoidal waveform is obtained by computer simulation of (1) with the parameters listed in Table 1, and initial states $x_1(0) = 300.002$ and $x_2(0) = 300.004$

The parameters chosen in this paper are summarized in Table 1. The 3D cross section of the surface $f_1(x_1, x_2, v)$ and $f_2(x_1, x_2, v)$ are shown in Fig. 2a and b respectively at $V = 6.4$ V. Although (1) can be implemented in hardware by several methods, all results in this paper are obtained by computer simulations to avoid ambiguities in modeling the physical devices.

2 Pinched Hysteresis Loop and DC V-I Curve of the Second-Order-Generic Memristor from Fig. 1c

2.1 Pinched Hysteresis Loops Under Bipolar Periodic Signal

The memristor exhibits a unique fingerprint called a pinched hysteresis loop under excitation of any bipolar periodic signal with zero average. To illustrate the

Table 1 Parameter values of the second-order generic memristor

| | |
|------------------|------------------|
| $K1 = 10^3$ | $K2 = 10^5$ |
| $\beta_1 = 10^4$ | $\beta_2 = 10^7$ |
| $\gamma_1 = 300$ | $\gamma_2 = 300$ |
| $\alpha_1 = 0.8$ | $\alpha_2 = 0.2$ |
| $\delta_1 = 0.8$ | $\delta_2 = 0.1$ |

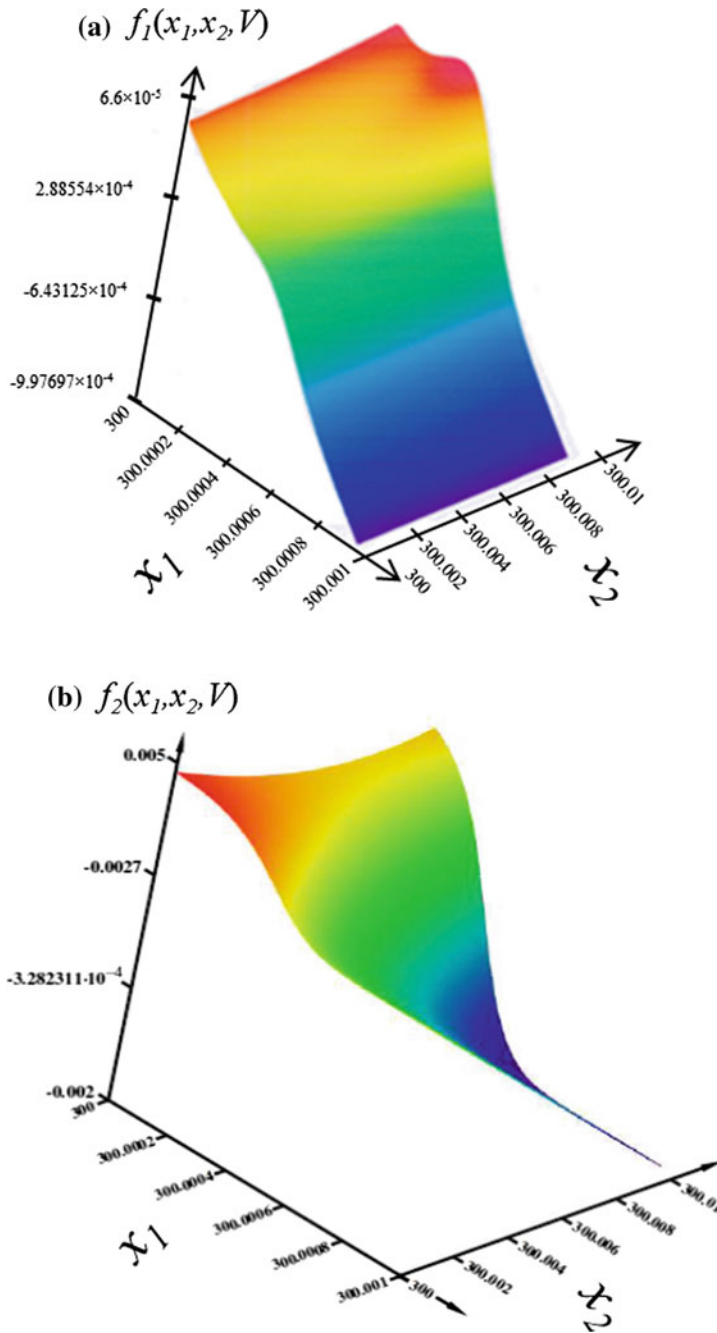


Fig. 2 The cross section of the surfaces **a** $f_1(x_1, x_2, V)$ and **b** $f_2(x_1, x_2, V)$ at $V = 6.4$ V

memristor in (1) exhibits this fingerprints, we apply a sinusoidal voltage signal $v(t) = A \sin(2\pi ft)$ with amplitude $A = 12$ V, and frequency $f = 0.1$ Hz across this memristor. Figure 3a shows the output current $i(t)$, the state variables $x_1(t)$, $x_2(t)$ and the memductance $G(t)$ with respect to time t , respectively. Observe from Fig. 3a that $i(t)$ always passes through the origin whenever $v(t)$ is zero at point 1, and 3. Observe also the memductance $G(t) \geq 0$. The upper figure in Fig. 3b is a double-valued Lissajous figure plotted on the i versus v plane. Such a multi-valued Lissajous figure of $v(t)$, $i(t)$, which passes through the origin is called a pinched hysteresis loop (Chua 2003). This unique feature is the characteristic property of a memristor that distinguishes it from non-memristive devices. The lower figure in Fig. 3b shows the variation of memductance with respect to applied voltage $v(t)$.

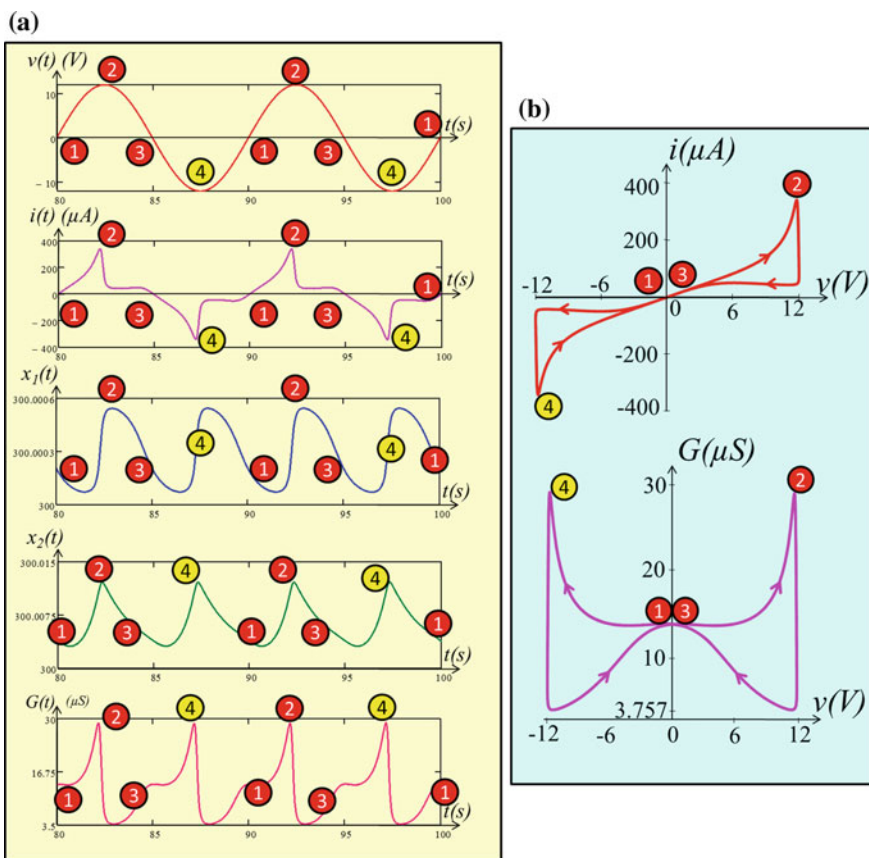
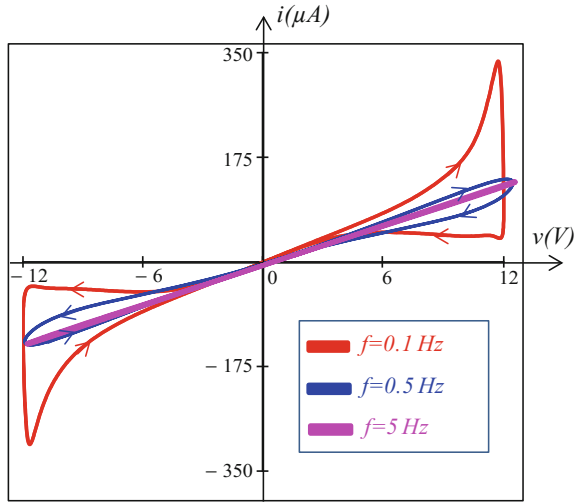


Fig. 3 **a** Waveforms of the applied sinusoidal voltage $v(t) = A \sin(2\pi ft)$, output current $i(t)$, state variables $x_1(t)$, $x_2(t)$, and memductance $G(t)$ of the second-order generic memristor. **b** Pinched hysteresis loop plotted on the i versus v plane and memductance hysteresis loop plotted on the G versus v plane, respectively. The simulations were performed at $A = 12$ V, $f = 0.1$ Hz, $x_1(0) = 300.002$ and $x_2(0) = 300.004$

Fig. 4 Pinched hysteresis loops of the second-order generic memristor at frequencies $f = 0.1, 0.5$ and 5 Hz. The input is a sinusoidal signal $v(t) = A \sin(2\pi ft)$, with $A = 12$ V, and the initial states are $x_1(0) = 300.002$ and $x_2(0) = 300.004$



Another characteristic property of the memristor is the dependence of the pinched hysteresis loop on the frequency of the excitation signal. This property asserts that the pinched hysteresis loops characterized by a memristor shrink to a single-value function through origin as the frequency tends to infinity. We illustrate this property by applying the sinusoidal signal $v(t) = A \sin(2\pi ft)$ with $A = 12$ V and $f = 0.1, 0.5$, and 5 Hz to our memristor. Observe from Fig. 4 that the pinched hysteresis loops shrink as the frequencies increase and tend to a straight line at 5 Hz (Adhikari et al. 2013; Mannan et al. 2016; Rajamani et al. 2016). All of these pinched hysteresis loops exhibit the fingerprints of a memristor.

2.2 DC V-I Curve

The DC V - I curve of a generic memristor is equivalent to a nonlinear resistor at the DC steady state regime (Chua 2014). The DC V - I curve of the second-order generic memristor defined in (1a)–(1d) is obtained by equating (1c) and (1d) to zero and solving for the equilibrium point as a function of applied DC voltage $v = V$, i.e.

$$x_1 = \hat{x}_1(V) \quad (2a)$$

$$x_2 = \hat{x}_2(V) \quad (2b)$$

Substituting (2a) and (2b) in (1b), and solving for the DC current $i = I$ from (1a), we obtain

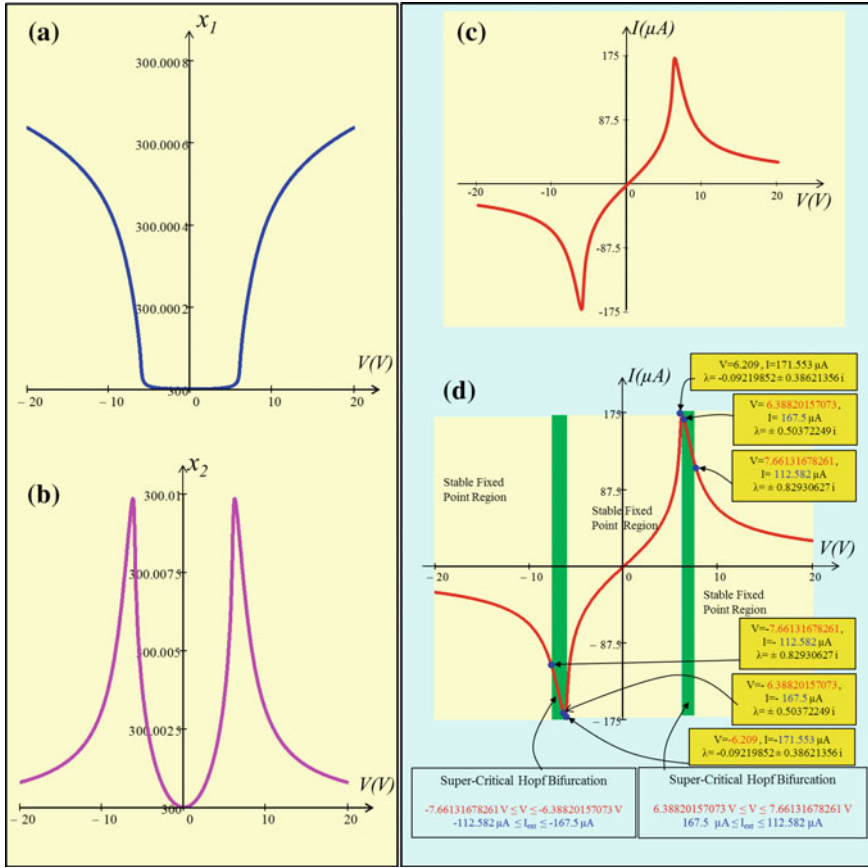


Fig. 5 The DC equilibrium of **a** state x_1 , **b** state x_2 , and **c** DC V - I curve in steady state regime, for $-20 \text{ V} \leq V \leq 20 \text{ V}$, **d** portions of the DC V - I curve which give rise to two distinct super-critical Hopf bifurcations

$$I = G(x_1, x_2) V \quad (3)$$

Applying (2a), (2b) and (3), for $-20 \text{ V} \leq V \leq 20 \text{ V}$, we obtain the red DC V - I curve of our second-order generic memristor shown in Fig. 5c whereas the state variables x_1 and x_2 are shown in Fig. 5a and b, respectively. Note that at *steady state* the V - I curve in Fig. 5c is equivalent to the V - I curve of a *nonlinear resistor* (Chua 1969). Figure 5d shows the portions of the DC V - I curve which give rise to two distinct super-critical Hopf bifurcations.

3 Small-Signal Equivalent Circuit

Small-signal equivalent circuit is the *linearized* circuit used to predict the response of a memristor to a *small-signal* input applied at an equilibrium point. Just like standard electronic circuit theory, the small-signal equivalent circuit is derived about an equilibrium point (V, I) by using the Taylor series and the Laplace transform. Let V be the DC voltage at an equilibrium point Q , then the equilibrium state $x_1 = X_1$ and $x_2 = X_2$ can be found by solving (1c) and (1d) numerically at the DC voltage V as follow:

$$\frac{dx_1}{dt} = \frac{1}{\alpha_1} \left[\delta_1(\gamma_1 - x_1) + \frac{K_1 e^{\beta_1(x_1 - \gamma_1)}}{\left((K_1 e^{\beta_1(x_1 - \gamma_1)}) + \left(K_2 e^{\beta_2\left(\frac{1}{x_2} - \frac{1}{\gamma_2}\right)} \right) \right)^2} V^2 \right] = 0 \quad (4a)$$

$$\frac{dx_2}{dt} = \frac{1}{\alpha_2} \left[\delta_2(\gamma_2 - x_2) + \frac{K_2 e^{\beta_2\left(\frac{1}{x_2} - \frac{1}{\gamma_2}\right)}}{\left((K_1 e^{\beta_1(x_1 - \gamma_1)}) + \left(K_2 e^{\beta_2\left(\frac{1}{x_2} - \frac{1}{\gamma_2}\right)} \right) \right)^2} V^2 \right] = 0 \quad (4b)$$

The memristance $M(x_1, x_2) \triangleq \frac{1}{G(x_1, x_2)}$ of the 2nd-order memristor defined in (1b) is composed of the following two decoupled terms involving only x_1 and x_2 , respectively:

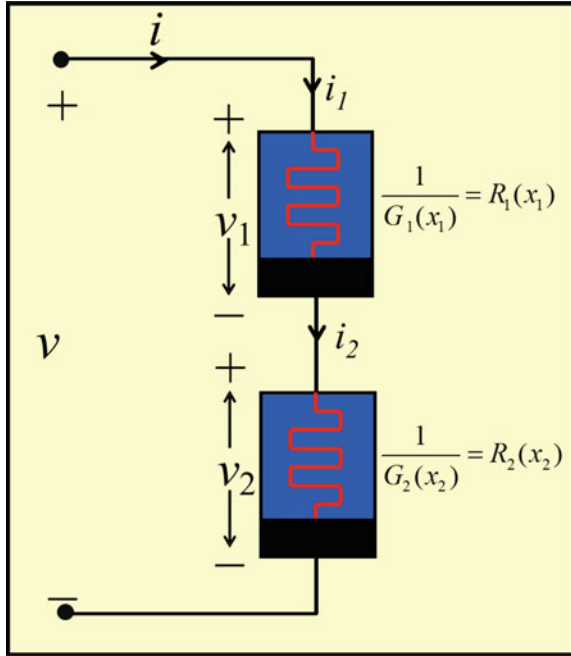
$$M(x_1, x_2) = \left(K_1 e^{\beta_1(x_1 - \gamma_1)} \right) + \left(K_2 e^{\beta_2\left(\frac{1}{x_2} - \frac{1}{\gamma_2}\right)} \right) \quad (5)$$

We can synthesize the $M(x_1, x_2)$ by two first-order memristors connected in series, as shown in Fig. 6. The memristance of the upper and lower memristors in Fig. 6 are defined by the first and second terms of Eq. (5) respectively, where the memductance $G_1(x_1) = 1/R_1(x_1)$ and $G_2(x_2) = 1/R_2(x_2)$ are defined in (6a) and (6b), respectively:

$$G_1(x_1) = \frac{1}{(K_1 e^{\beta_1(x_1 - \gamma_1)})} \quad (6a)$$

$$G_2(x_2) = \frac{1}{K_2 e^{\beta_2\left(\frac{1}{x_2} - \frac{1}{\gamma_2}\right)}} \quad (6b)$$

Fig. 6 The second-order memristor defined in (1) can be realized by connecting two “uncoupled” first-order voltage-controlled memristors in series. The memductance $G_1(x_1)$ of the first memristor is defined by (6a), and the memductance $G_2(x_2)$ of the second memristor is defined by (6b). The corresponding state equation is given by (9) and (10), respectively



Note that $i = i_1 = i_2$ and $v = v_1 + v_2$ in Fig. 6. Using (6a) and (6b), we have following relationships:

$$G_1(x_1)v_1 = G_2(x_2)v_2 \quad (7a)$$

$$v_1 + v_2 = v \quad (7b)$$

It follows from (7a) and (7b) that

$$v = \frac{G_1(x_1) + G_2(x_2)}{G_2(x_2)} v_1 \quad (7c)$$

$$= \left(\frac{K_1 e^{\beta_1(x_1 - \gamma_1)} + K_2 e^{\beta_2 \left(\frac{1}{x_2} - \frac{1}{\gamma_2} \right)}}{K_1 e^{\beta_1(x_1 - \gamma_1)}} \right) v_1 \quad (8)$$

From (8) and (1c), we obtain the following state equation of the upper memristor:

$$\frac{dx_1}{dt} = \frac{1}{\alpha_1} \left[\delta_1(\gamma_1 - x_1) + \frac{1}{K_1 e^{\beta_1(x_1 - \gamma_1)}} v_1^2 \right] \triangleq f(x_1, v_1) \quad (9)$$

A similar derivation with respect to v_2 gives the following state equation for the lower memristor:

$$\frac{dx_2}{dt} = \frac{1}{\alpha_2} \left[\delta_2(\gamma_2 - x_2) + \frac{1}{K_2 e^{\beta_2 \left(\frac{1}{x_2} - \frac{1}{\gamma_2} \right)}} v_2^2 \right] \triangleq f(x_2, v_2) \quad (10)$$

Let us derive small-signal equivalent circuit of the upper and lower memristor in Fig. 6 at their DC equilibrium point $v_I = V_I$ and $v_2 = V_2$ where $V_I + V_2 = V$. Define,

$$x_1 = X_I + \delta x_1 \quad (11a)$$

$$v_1 = V_I + \delta v_1 \quad (11b)$$

$$i_1 = I_I + \delta i_1 \quad (11c)$$

where X_I denotes the equilibrium state $x_I(Q)$ of the upper memristor at $v_I = V_I$.

We can expand the current i_I due to the memductance $G_1(x_I)$ in a Taylor series about the equilibrium point $x_I = X_I$ as follows:

$$\begin{aligned} i_1 &= I_I + \delta i_1 \\ &= a'_{00}(Q) + a'_{11}(Q)\delta x_1 + a'_{12}(Q)\delta v_1 + h.o.t \end{aligned} \quad (12a)$$

where,

$$I_I = a'_{00}(Q) = G_1(X_I)V_I \quad (12b)$$

$$a'_{11}(Q) = \dot{G}_1(x_1)v_1|_Q = -\beta_1 \left(K_1 e^{\beta_1(X_I - \gamma_1)} \right)^{-1} V_I \quad (12c)$$

$$a'_{12}(Q) = G_1(x_1)|_Q = \left(K_1 e^{\beta_1(X_I - \gamma_1)} \right)^{-1} \quad (12d)$$

and $h.o.t$ denotes the higher-order terms in δx_1 and δv_1 . Assuming $|\delta x_1| \ll 1$ and $|\delta v_1| \ll 1$, we can neglect the $h.o.t$ term in (12a) to obtain the following *linear* equation,

$$\delta i_1 = a'_{11}(Q)\delta x_1 + a'_{12}(Q)\delta v_1 \quad (13)$$

Let us expand state equation $f(x_1, v_1)$ of (9) in Taylor series about the equilibrium point $(x_I(Q), V_I(Q))$:

$$f(X_1 + \delta x_1, V_1 + \delta v_1) = f(X_1, V_1) + b_{11}(Q)\delta x_1 + b_{12}(Q)\delta v_1 + h.o.t \quad (14a)$$

where,

$$b'_{11}(Q) = \left. \frac{\partial f(x_1, v_1)}{\partial x_1} \right|_Q = - \left[\frac{\delta_1}{\alpha_1} + \frac{\beta_1 V_1^2}{\alpha_1} \left(K_1 e^{\beta_1 (X_1 - \gamma_1)} \right)^{-1} \right] \quad (14b)$$

$$b'_{12}(Q) = \left. \frac{\partial f(x_1, v_1)}{\partial v_1} \right|_Q = \frac{2(K_1 e^{\beta_1 (X_1 - \gamma_1)})^{-1}}{\alpha_1} V_1 \quad (14c)$$

Note that $f(X_1, V_1) = 0$ since (X_1, V_1) is a point on the DC $V_1 - I_1$ curve. Let us linearize the non-linear state equation $\dot{x}_1 = f(x_1, v_1)$ by neglecting the *h.o.t* from (14a) as follows:

$$\frac{d(\delta x_1)}{dt} = b'_{11}(Q)\delta x_1 + b'_{12}(Q)\delta v_1 \quad (15)$$

Taking the Laplace transform of (13) and (15) (Chua and Kang 1976) we obtain,

$$\hat{i}_1(s) = a'_{11}(Q)\hat{x}_1(s) + a'_{12}(Q)\hat{v}_1(s) \quad (16)$$

$$s\hat{x}_1(s) = b'_{11}(Q)\hat{x}_1(s) + b'_{12}(Q)\hat{v}_1(s) \quad (17)$$

where the Laplace transform of $\delta x_1(t)$, $\delta i_1(t)$ and $\delta v_1(t)$ are denoted by $\hat{x}_1(s)$, $\hat{i}_1(s)$ and $\hat{v}_1(s)$ respectively. From (17), we obtain

$$\hat{x}_1(s) = \frac{b'_{12}(Q)\hat{v}_1(s)}{s - b'_{11}(Q)} \quad (18)$$

From (16) and (18), the admittance function $Y_1(s, Q)$ of the upper memristor is

$$Y_1(s, Q) \triangleq \frac{\hat{i}_1(s)}{\hat{v}_1(s)} = \frac{a'_{11}(Q)b'_{12}(Q)}{s - b'_{11}(Q)} + a'_{12}(Q) \quad (19)$$

Rearranging (19), we obtain

$$Y_1(s, Q) = \frac{1}{s \frac{1}{a'_{11}(Q)b'_{12}(Q)} + \frac{(-b'_{11}(Q))}{a'_{11}(Q)b'_{12}(Q)}} + a'_{12}(Q) \quad (20)$$

Let us recast (20) into the form

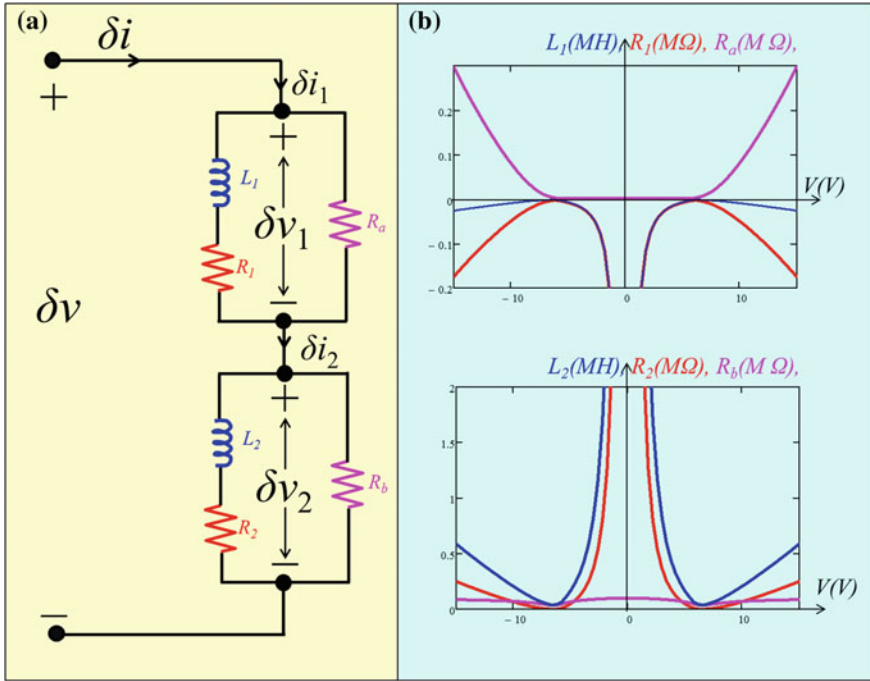


Fig. 7 **a** Small-signal equivalent circuit of the second-order memristor. **b** Inductances and resistances in the small-signal equivalent circuit of the second-order memristor calculated at the DC voltage V

$$Y_1(s, Q) = \frac{1}{sL_1 + R_1} + \frac{1}{R_a} \quad (21)$$

where $Y_1(s, Q)$ denotes the small-signal admittance of the upper memristor at Q , whose circuit as shown in Fig. 7a, where the parameters L_1 , R_1 and R_a are defined by:

$$L_1 = \frac{1}{a'_{11}(Q)b'_{12}(Q)} \quad (22a)$$

$$R_1 = \frac{-b'_{11}(Q)}{a'_{11}(Q)b'_{12}(Q)} \quad (22b)$$

$$R_a = \frac{1}{a'_{12}(Q)} \quad (22c)$$

and state variable x_1 at Q can be computed numerically by solving the following equation:

$$\frac{dx_1}{dt} = \frac{1}{\alpha_1} [\delta_1(\gamma_1 - x_1) + G_1(x_1)V_1^2] = 0 \quad (22d)$$

Similarly, the small-signal admittance of the lower memristor is given by

$$Y_2(s, Q) \triangleq \frac{\hat{i}_2(s)}{\hat{v}_2(s)} = \frac{c'_{11}(Q)d'_{12}(Q)}{s - d'_{11}(Q)} + c'_{12}(Q) \quad (23)$$

Rearranging (23), we have

$$Y_2(s, Q) = \frac{1}{s \frac{1}{c'_{11}(Q)d'_{12}(Q)} + \frac{(-d'_{11}(Q))}{c'_{11}(Q)d'_{12}(Q)}} + c'_{12}(Q) = \frac{1}{sL_2 + R_2} + \frac{1}{R_b} \quad (24)$$

where $Y_2(s, Q)$ denotes the small-signal admittance of the lower memristor of the circuit of Fig. 7a where the parameters L_2 , R_2 and R_b are given by:

$$L_2 = \frac{1}{c'_{11}(Q)d'_{12}(Q)} \quad (25a)$$

$$R_2 = \frac{-d'_{11}(Q)}{c'_{11}(Q)d'_{12}(Q)} \quad (25b)$$

$$R_b = \frac{1}{c'_{12}(Q)} \quad (25c)$$

The state variable x_2 at the equilibrium point Q can be computed numerically by solving the following equation:

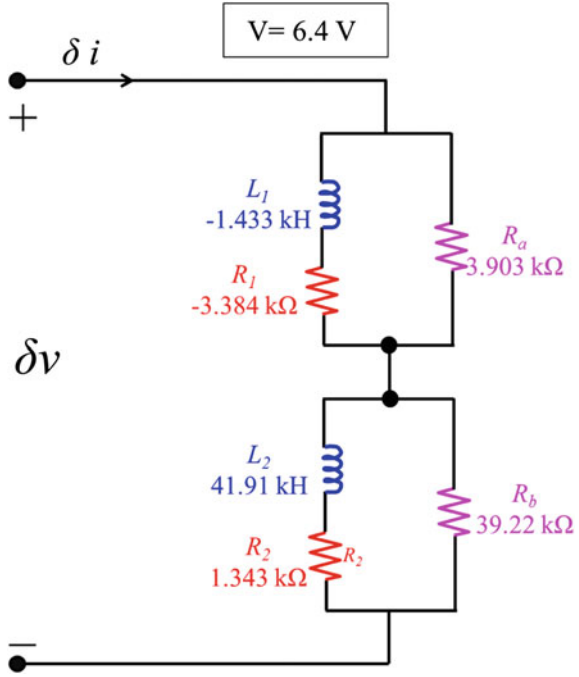
$$\frac{dx_2}{dt} = \frac{1}{\alpha_2} [\delta_2(\gamma_2 - x_2) + G_2(x_2)V_2^2] = 0 \quad (25d)$$

For the convenience of readers, the explicit formulas for computing L_l , R_l , R_a and L_2 , R_2 , R_b as a function of V_1 and V_2 are given in Table 2 along with the state equations $f(x_1, v_1)$ and $f(x_2, v_2)$, respectively. The corresponding small-signal equivalent circuit due to L_l , R_l , R_a and L_2 , R_2 , R_b and plots of inductances and resistances are shown in Fig. 7a and b, respectively, for the memristor. Observe that the inductance L_l and resistance R_l are always negative for any DC equilibrium voltage V . The small-signal equivalent circuit of the second-order generic memristor with its inductances and resistances calculated at $V = 6.4$ V is shown in Fig. 8.

Table 2 Formulas for calculating L_1 , R_1 , R_a and L_2 , R_2 , R_b of the second-order memristor

| Computation of L_1 | Computation of R_1 | Computation of R_a and x_1 |
|---|--|---|
| $a'_{11}(Q) = \dot{G}_1(x_1)v_1 _Q$ $G_1(x_1) = \left(K_1 e^{\beta_1(x_1 - \gamma_1)}\right)^{-1}$ $\dot{G}_1(x_1) _Q = -\frac{\beta_1}{K_1 e^{\beta_1(x_1 - \gamma_1)}}$ $a'_{11}(Q) = -\frac{\beta_1}{K_1 e^{\beta_1(x_1 - \gamma_1)}} V_1$ $b'_{12}(Q) = \frac{\partial f(x_1, v_1)}{\partial v_1} \Big _Q$ $= \frac{2G_1(x_1)}{\alpha_1} V_1$ $L_1 = \frac{1}{a'_{11}(Q)b'_{12}(Q)}$ | $b'_{11}(Q) = \frac{\partial f(x_1, v_1)}{\partial x_1} \Big _Q$ $= -\left[\frac{\delta_1}{\alpha_1} + \frac{\beta_1 V_1^2}{\alpha_1} \left(K_1 e^{\beta_1(x_1 - \gamma_1)}\right)^{-1}\right]$ $R_1 = -\frac{b'_{11}(Q)}{a'_{11}(Q)b'_{12}(Q)}$ | $a'_{12}(Q) = G_1(x_1) _Q$ $= \left(K_1 e^{\beta_1(x_1 - \gamma_1)}\right)^{-1}$ $R_a = \frac{1}{a'_{12}(Q)}$ <p>Numerically, x_1 can be computed as</p> $\frac{dx_1}{dt} = \frac{1}{\alpha_1} [\delta_1 (\gamma_1 - x_1) + G_1(x_1)V_1^2] = 0$ |
| Computation of L_2 | Computation of R_2 | Computation of R_b and x_2 |
| $c'_{11}(Q) = \dot{G}_2(x_2)v_2 _Q$ $G_2(x_2) = \left(K_2 e^{\beta_2\left(\frac{1}{x_2} - \frac{1}{\gamma_2}\right)}\right)^{-1}$ $\dot{G}_2(x_2) _Q = \frac{\beta_2}{K_2 x_2^2} \left(e^{\beta_2\left(\frac{1}{x_2} - \frac{1}{\gamma_2}\right)}\right)^{-1}$ $c'_{11}(Q) = \frac{\beta_2}{K_2 x_2^2} \left(e^{\beta_2\left(\frac{1}{x_2} - \frac{1}{\gamma_2}\right)}\right)^{-1} V_2$ $d'_{12}(Q) = \frac{\partial f(x_2, v_2)}{\partial v_2} \Big _Q$ $= \frac{2G_2(x_2)}{\alpha_2} V_2$ $L_2 = \frac{1}{c'_{11}(Q)d'_{12}(Q)}$ | $d'_{11}(Q) = \frac{\partial f(x_2, v_2)}{\partial x_2} \Big _Q$ $= \left(-\frac{\delta_2}{\alpha_2} + \left(\frac{\beta_2 V_2^2}{K_2 \alpha_2 x_2^2} \left(e^{\beta_2\left(\frac{1}{x_2} - \frac{1}{\gamma_2}\right)}\right)^{-1}\right)\right)$ $R_2 = -\frac{d'_{11}(Q)}{c'_{11}(Q)d'_{12}(Q)}$ | $c'_{12}(Q) = G_2(x_2) _Q$ $= \left(K_2 e^{\beta_2\left(\frac{1}{x_2} - \frac{1}{\gamma_2}\right)}\right)^{-1}$ $R_b = \frac{1}{c'_{12}(Q)}$ <p>Numerically, x_2 can be computed as</p> $\frac{dx_2}{dt} = \frac{1}{\alpha_2} [\delta_2 (\gamma_2 - x_2) + G_2(x_2)V_2^2] = 0$ |

Fig. 8 Small-signal equivalent circuit of the second-order generic memristor calculated at $V = 6.4$ V



3.1 Admittance and Pole-Zero Diagram of Second-Order Memristor

Let $Q(V_Q, I_Q)$ be any point on the DC V - I curve of a second-order generic memristor and let (X_{1Q}, X_{2Q}) be the corresponding equilibrium state.

Define,

$$x_1 = X_{1Q} + \Delta x_1 \quad (26a)$$

$$x_2 = X_{2Q} + \Delta x_2 \quad (26b)$$

$$v = V_Q + \Delta v \quad (26c)$$

$$i = I_Q + \Delta i \quad (26d)$$

Let us expand the current $i = G(x_1, x_2) v$ in (1a) using Taylor series at the equilibrium point (X_{1Q}, X_{2Q}, V_Q)

$$i = a_{00} + a_{11}\Delta x_1 + a_{12}\Delta x_2 + a_{13}\Delta v + h.o.t. \quad (27)$$

where,

$$a_{00} = G(X_{1_Q}, X_{2_Q}) V_Q = I_Q \quad (28a)$$

$$a_{11} = V_Q \left. \frac{\partial G(x_1, x_2)}{\partial x_1} \right|_Q \quad (28b)$$

$$a_{12} = V_Q \left. \frac{\partial G(x_1, x_2)}{\partial x_2} \right|_Q \quad (28c)$$

$$a_{13} = G(x_1, x_2)|_Q = G(X_{1_Q}, X_{2_Q}) \quad (28d)$$

The h.o.t. in (27) denotes the higher-order terms of Δx_I , Δx_2 , and Δv_I . Assuming $\Delta x_I \ll 1$, $\Delta x_2 \ll 1$ and $\Delta v_I \ll 1$ then the h.o.t. term can be neglected and (27) reduces to the following linear equation

$$\boxed{\Delta i = a_{11} \Delta x_1 + a_{12} \Delta x_2 + a_{13} \Delta v} \quad (29)$$

Let us expand $f_I(x_I, x_2, v)$ in (1c) using Taylor series at the equilibrium point (X_{1_Q}, X_{2_Q}, V_Q)

$$f_I(X_{1_Q} + \Delta x_1, X_{2_Q} + \Delta x_2, V_Q + \Delta v) = f_I(X_{1_Q}, X_{2_Q}, V_Q) + b_{11} \Delta x_1 + b_{12} \Delta x_2 + b_{13} \Delta v + h.o.t. \quad (30)$$

where,

$$b_{11} = \left. \frac{\partial f_I(x_1, x_2, v)}{\partial x_1} \right|_Q \quad (31a)$$

$$b_{12} = \left. \frac{\partial f_I(x_1, x_2, v)}{\partial x_2} \right|_Q \quad (31b)$$

$$b_{13} = \left. \frac{\partial f_I(x_1, x_2, v)}{\partial v} \right|_Q \quad (31c)$$

Since (X_{1_Q}, X_{2_Q}, V_Q) specifies a point on the DC V - I curve, the term $f_I(X_{1_Q}, X_{2_Q}, V_Q) = 0$. Neglecting the h.o.t. term in (30), we obtain the following linear equation:

$$\boxed{\frac{d(\Delta x_1)}{dt} = b_{11} \Delta x_1 + b_{12} \Delta x_2 + b_{13} \Delta v} \quad (32)$$

Similarly, let us expand $f_2(x_I, x_2, v)$ in (1d) using Taylor series at the equilibrium point (X_{1_Q}, X_{2_Q}, V_Q)

$$f_2(X_{1_Q} + \Delta x_1, X_{2_Q} + \Delta x_2, V_Q + \Delta v) = f_2(X_{1_Q}, X_{2_Q}, V_Q) + c_{11}\Delta x_1 + c_{12}\Delta x_2 + c_{13}\Delta v + h.o.t. \quad (33)$$

where,

$$c_{11} = \left. \frac{\partial f_2(x_1, x_2, v)}{\partial x_1} \right|_Q \quad (34a)$$

$$c_{12} = \left. \frac{\partial f_2(x_1, x_2, v)}{\partial x_2} \right|_Q \quad (34b)$$

$$c_{13} = \left. \frac{\partial f_2(x_1, x_2, v)}{\partial v} \right|_Q \quad (34c)$$

Since (X_{1_Q}, X_{2_Q}, V_Q) specifies a point on the DC V - I curve, the term $f_2(X_{1_Q}, X_{2_Q}, V_Q) = 0$. Neglecting the h.o.t. term in (33), we obtain the following linear equation:

$$\boxed{\frac{d(\Delta x_2)}{dt} = c_{11}\Delta x_1 + c_{12}\Delta x_2 + c_{13}\Delta v} \quad (35)$$

Taking Laplace transform of (29), (32) and (35), we obtain

$$\hat{i}(s) = a_{11}\hat{x}_1(s) + a_{12}\hat{x}_2(s) + a_{13}\hat{v}(s) \quad (36)$$

$$s\hat{x}_1(s) = b_{11}\hat{x}_1(s) + b_{12}\hat{x}_2(s) + b_{13}\hat{v}(s) \quad (37)$$

$$s\hat{x}_2(s) = c_{11}\hat{x}_1(s) + c_{12}\hat{x}_2(s) + c_{13}\hat{v}(s) \quad (38)$$

where $\hat{i}(s)$, $\hat{x}_1(s)$, $\hat{x}_2(s)$ and $\hat{v}(s)$ denote the Laplace transform of Δi , Δx_1 , Δx_2 , and Δv , respectively. Solving (37) and (38) for $\hat{x}_1(s)$ and $\hat{x}_2(s)$, we obtain

$$\hat{x}_1(s) = \frac{[b_{12}c_{13} + b_{13}(s - c_{12})]}{[(s - b_{11})(s - c_{12}) - b_{12}c_{11}]} \hat{v}(s) \quad (39a)$$

$$\hat{x}_2(s) = \frac{[b_{13}c_{11} + c_{13}(s - b_{11})]}{[(s - b_{11})(s - c_{12}) - b_{12}c_{11}]} \hat{v}(s) \quad (39b)$$

The explicit formula for computing the parameters in (39a) and (39b) are given in Table 3. By substituting $\hat{x}_1(s)$ and $\hat{x}_2(s)$ from (39a, 39b) into (36), we obtain

$$Y(s; Q) \triangleq \frac{\hat{i}(s)}{\hat{v}(s)} \quad (40)$$

Table 3 Explicit formula for computing the parameters in (40)

| | |
|--|---|
| $a_{11} = \frac{-V K_1 \beta_1 e^{\beta_1 (X_1 - \gamma_1)}}{\left[\left(K_1 e^{\beta_1 (X_1 - \gamma_1)} \right) + \left(K_2 e^{\beta_2 \left(\frac{1}{X_2} - \frac{1}{\gamma_2} \right)} \right) \right]^2}$ | |
| $a_{12} = \frac{V K_2 \beta_2 e^{\beta_2 \left(\frac{1}{X_2} - \frac{1}{\gamma_2} \right)}}{X_2^2 \left[\left(K_1 e^{\beta_1 (X_1 - \gamma_1)} \right) + \left(K_2 e^{\beta_2 \left(\frac{1}{X_2} - \frac{1}{\gamma_2} \right)} \right) \right]^2}$ | |
| $a_{13} = \frac{1}{\left(K_1 e^{\beta_1 (X_1 - \gamma_1)} \right) + \left(K_2 e^{\beta_2 \left(\frac{1}{X_2} - \frac{1}{\gamma_2} \right)} \right)}$ | |
| $b_{11} = \frac{-1}{\alpha_1} \left[\delta_1 - \frac{K_1 \beta_1 e^{\beta_1 (X_1 - \gamma_1)}}{\left(\left(K_1 e^{\beta_1 (X_1 - \gamma_1)} \right) + \left(K_2 e^{\beta_2 \left(\frac{1}{X_2} - \frac{1}{\gamma_2} \right)} \right) \right)^2} V^2 + \frac{2 K_1^2 \beta_1 e^{2 \beta_1 (X_1 - \gamma_1)}}{\left(\left(K_1 e^{\beta_1 (X_1 - \gamma_1)} \right) + \left(K_2 e^{\beta_2 \left(\frac{1}{X_2} - \frac{1}{\gamma_2} \right)} \right) \right)^3} V^2 \right]$ | |
| $b_{12} = \frac{2 K_1 K_2 \beta_2 e^{\beta_2 \left(\frac{1}{X_2} - \frac{1}{\gamma_2} \right)}}{\alpha_1 X_2^2 \left[\left(K_1 e^{\beta_1 (X_1 - \gamma_1)} \right) + \left(K_2 e^{\beta_2 \left(\frac{1}{X_2} - \frac{1}{\gamma_2} \right)} \right) \right]^3} V^2$ | $b_{13} = \frac{2 K_1 e^{\beta_1 (X_1 - \gamma_1)}}{\alpha_1 \left[\left(K_1 e^{\beta_1 (X_1 - \gamma_1)} \right) + \left(K_2 e^{\beta_2 \left(\frac{1}{X_2} - \frac{1}{\gamma_2} \right)} \right) \right]^2} V$ |
| $c_{11} = \frac{-2 K_1 K_2 \beta_1 e^{\beta_1 (X_1 - \gamma_1)} e^{\beta_2 \left(\frac{1}{X_2} - \frac{1}{\gamma_2} \right)}}{\alpha_2 \left[\left(K_1 e^{\beta_1 (X_1 - \gamma_1)} \right) + \left(K_2 e^{\beta_2 \left(\frac{1}{X_2} - \frac{1}{\gamma_2} \right)} \right) \right]^3} V^2$ | $c_{13} = \frac{2 K_2 e^{\beta_2 \left(\frac{1}{X_2} - \frac{1}{\gamma_2} \right)}}{\alpha_2 \left[\left(K_1 e^{\beta_1 (X_1 - \gamma_1)} \right) + \left(K_2 e^{\beta_2 \left(\frac{1}{X_2} - \frac{1}{\gamma_2} \right)} \right) \right]^2} V$ |
| $c_{12} = \frac{-1}{\alpha_2} \left[\delta_2 + \frac{K_2 \beta_2 e^{\beta_2 \left(\frac{1}{X_2} - \frac{1}{\gamma_2} \right)}}{X_2^2 \left[\left(K_1 e^{\beta_1 (X_1 - \gamma_1)} \right) + \left(K_2 e^{\beta_2 \left(\frac{1}{X_2} - \frac{1}{\gamma_2} \right)} \right) \right]^2} V^2 - \frac{2 K_2^2 \beta_2 e^{2 \beta_2 \left(\frac{1}{X_2} - \frac{1}{\gamma_2} \right)}}{X_2^2 \left[\left(K_1 e^{\beta_1 (X_1 - \gamma_1)} \right) + \left(K_2 e^{\beta_2 \left(\frac{1}{X_2} - \frac{1}{\gamma_2} \right)} \right) \right]^3} V^2 \right]$ | |
| $x_1 = X_1 \text{ and } x_2 = X_2 \text{ can be computed by solving the following equilibrium equations at } V$ | |
| $\delta_1 (\gamma_1 - x_1) + \frac{K_1 e^{\beta_1 (x_1 - \gamma_1)}}{\left(\left(K_1 e^{\beta_1 (x_1 - \gamma_1)} \right) + \left(K_2 e^{\beta_2 \left(\frac{1}{x_2} - \frac{1}{\gamma_2} \right)} \right) \right)^2} V^2 = 0$ | $\delta_2 (\gamma_2 - x_2) + \frac{K_2 e^{\beta_2 \left(\frac{1}{x_2} - \frac{1}{\gamma_2} \right)}}{\left(\left(K_1 e^{\beta_1 (x_1 - \gamma_1)} \right) + \left(K_2 e^{\beta_2 \left(\frac{1}{x_2} - \frac{1}{\gamma_2} \right)} \right) \right)^2} V^2 = 0$ |

$$Y(s; Q) = \frac{b_2 s^2 + b_1 s + b_0}{a_2 s^2 + a_1 s + a_0} \quad (41)$$

The expression $Y(s; Q)$ in (41) is called the small-signal admittance of the second-order memristor about the equilibrium point Q , where a_2, a_1, a_0, b_2, b_1 and b_0 are given by

$$\left. \begin{aligned} a_2 &= 1 \\ a_1 &= -(b_{11} + c_{12}) \\ a_0 &= b_{11}c_{12} - b_{12}c_{11} \end{aligned} \right\} \quad (42a)$$

$$\left. \begin{aligned} b_2 &= a_{13} \\ b_1 &= a_{11}b_{13} + a_{12}c_{13} - a_{13}(b_{11} + c_{12}) \\ b_0 &= a_{11}(b_{12}c_{13} - b_{13}c_{12}) + a_{12}(b_{13}c_{11} - b_{11}c_{13}) + a_{13}(b_{11}c_{12} - b_{12}c_{11}) \end{aligned} \right\} \quad (42b)$$

The *pole-zero diagram* of the small-signal admittance $Y(s; V)$ is computed by factorizing the denominator and numerator of (41):

$$Y(s; V) = \frac{k(s - z_1)(s - z_2)}{(s - p_1)(s - p_2)} \quad (43)$$

where p_i and z_i denote the poles and zeros of admittance function $Y(s; V)$ respectively.

The loci of the zeros and poles are shown in the Fig. 9a and b respectively, over the applied DC voltage $-20 \text{ V} \leq V \leq 20 \text{ V}$. In Fig. 9b, the arrowheads indicate the direction of pole movements in the interval of $-20 \text{ V} \leq V \leq 0 \text{ V}$ whereas the direction of pole movements for $0 \text{ V} \leq V \leq 20 \text{ V}$ is in reverse direction. Note that the reverse arrowheads for $0 \text{ V} \leq V \leq 20 \text{ V}$ are omitted to avoid the clutter.

Observe from Fig. 9a that $Im z_1, Im z_2$ are always zero, and $Re z_2$ is always negative. The poles diagram in Fig. 9b shows the real part of the poles p_1 and p_2 are zero at $V = 6.38820157073 \text{ V}$ and $V = 7.66131678261 \text{ V}$, respectively which are also called as *Hopf-bifurcation points* in bifurcation theory. Observe that the real parts Rep_1 and Rep_2 of the poles are always positive between the bifurcation points $6.38820157073 \text{ V} < V < 7.66131678261 \text{ V}$. In the horizontal segment where the $Im p_1$ and $Im p_2$ are zero, at that point several poles of Rep_1 and Rep_2 exist due to different input voltages as shown in Fig. 9b and at $V = 0 \text{ V}$, the value of Rep_1 and Rep_2 is -0.5 and -1 , respectively. As the value of the voltage V increases the value of the poles of p_1 and p_2 increases. For $V \leq 6.03481 \text{ V}$ and $V \geq 11.1305 \text{ V}$ the $Im p_1$ and $Im p_2$ become zero.

3.2 Frequency Response of Second-Order Generic Memristor

The frequency response of the second-order generic memristor at an equilibrium point Q is computed by substituting $s = i\omega$, for the complex frequency s in (41) at the equilibrium point Q , where the angular frequency $\omega = 2\pi f$. The corresponding

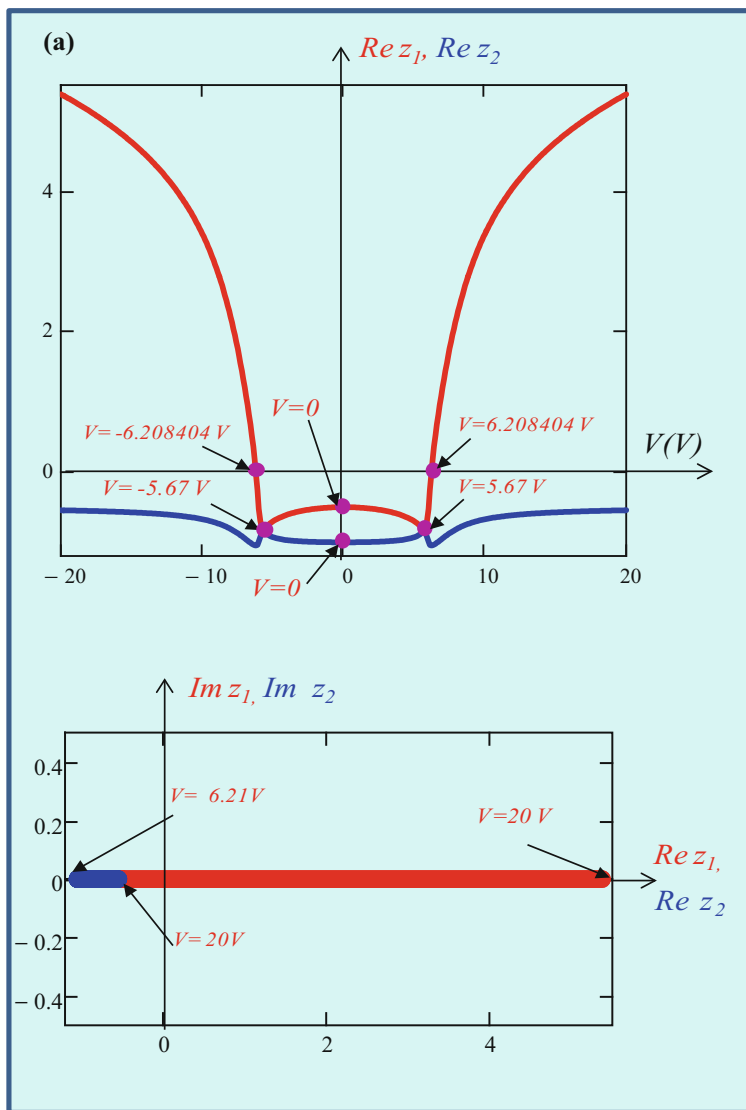


Fig. 9 Poles and zeros diagram of the admittance function $Y(s; V) = \frac{k(s - z_1)(s - z_2)}{(s - p_1)(s - p_2)}$ for $-20 \text{ V} \leq V \leq 20 \text{ V}$. **a** Zeros Diagram. **b** Poles Diagram. Arrowheads indicate the direction of pole movements in the interval of $-20 \text{ V} \leq V \leq 0 \text{ V}$. The movements of poles in the interval of $0 \text{ V} \leq V \leq 20 \text{ V}$, which are the reverse direction of $-20 \text{ V} \leq V \leq 0 \text{ V}$ interval, are omitted to avoid the clutter. When voltage V is infinitive, the locations of poles p_1 and p_2 are -0.5 and -77.4759895 , respectively

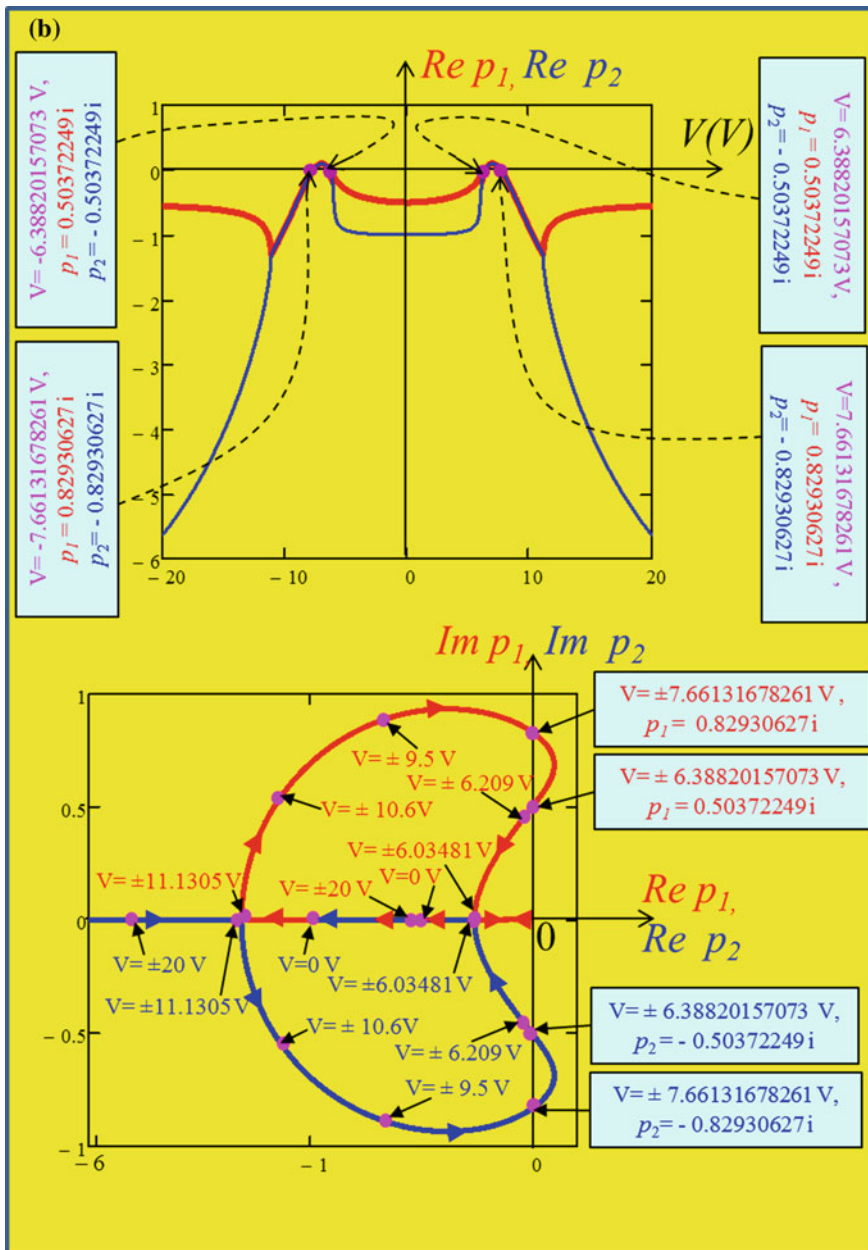


Fig. 9 (continued)

real part $\text{Re}Y(i\omega; V_Q)$ and imaginary part $\text{Im}Y(i\omega; V_Q)$ obtained from the admittance function $Y(i\omega; V_Q)$ are called the *small-signal admittance frequency response* of the memristor in basic circuit theory. When the function $\text{Re}Y(i\omega; V_Q)$ and $\text{Im}Y(i\omega; V_Q)$ are plotted on the horizontal and vertical axes of the Cartesian co-ordinate system with the frequency ω as a parameter, the resulting plot is generally known as *Nyquist plot* of the admittance functions at the equilibrium point Q .

Substituting $s = i\omega$ in (41), we obtain

$$Y(i\omega; V_Q) = \left[\frac{(a_0 - a_2\omega^2)(b_0 - b_2\omega^2) + a_1b_1\omega^2}{(a_0 - a_2\omega^2)^2 + a_1^2\omega^2} \right] + i \left[\frac{[(a_0 - a_2\omega^2)b_1 - a_1(b_0 - b_2\omega^2)]\omega}{(a_0 - a_2\omega^2)^2 + a_1^2\omega^2} \right] \quad (44)$$

The real and imaginary parts of the small-signal admittance $Y(i\omega; V_Q)$ at the equilibrium point $V_Q (X_{1_Q}, X_{2_Q})$ of a second-order generic memristor are given by:

$$\begin{aligned} \text{Re}Y(i\omega; V_Q) &= \frac{(a_0 - a_2\omega^2)(b_0 - b_2\omega^2) + a_1b_1\omega^2}{(a_0 - a_2\omega^2)^2 + a_1^2\omega^2} \\ \text{Im}Y(i\omega; V_Q) &= \frac{[(a_0 - a_2\omega^2)b_1 - a_1(b_0 - b_2\omega^2)]\omega}{(a_0 - a_2\omega^2)^2 + a_1^2\omega^2} \end{aligned} \quad (45)$$

By extensive numerical analysis of DC V - I curve shown in Fig. 5d, we found the current $I = 171.553 \mu\text{A}$ is the maximum value at $V = 6.209 \text{ V}^2$ and our calculation shows that the slope of DC V - I curve is negative when $V > 6.209 \text{ V}$. Figure 10a-c shows the admittance frequency response $\text{Re}Y(i\omega; V_Q)$ versus ω , $\text{Im}Y(i\omega; V_Q)$ versus ω and the *Nyquist plot* of the second-order memristor at $V = 6.209 \text{ V}$, $V = 6.3 \text{ V}$, and $V = 7 \text{ V}$, respectively. Observe that the function $\text{Re}Y(i\omega; V_Q)$ is tangent to the ω axis at $\omega = 0$ at $V = 6.209 \text{ V}$. However, the function $\text{Re}Y(i\omega; V_Q)$ at $V = 6.3 \text{ V}$ and $V = 7 \text{ V}$ are negative for $-0.42 \leq \omega \leq 0.42$, and $-0.6908 \leq \omega \leq 0.6908$, memristor defined in (1) is *locally active* when the DC input voltage $V > 6.209 \text{ V}$.

4 Mapping the Poles of the Admittance Function $Y(S; V)$ with Eigen values of the Jacobian Matrix $J(X_1, X_2; V)$

Let us represent (1c) and (1d) with DC input voltage V in the following standard form:

$$\frac{dx_1}{dt} = f_1(x_1, x_2, V) \quad (46a)$$

²The DC V - I curve in Fig. 5d for negative voltage ($V \leq 0$) is just the reflected (odd-symmetric) mirror image about the origin $V = 0$ over the positive input voltage ($V \geq 0$) region.

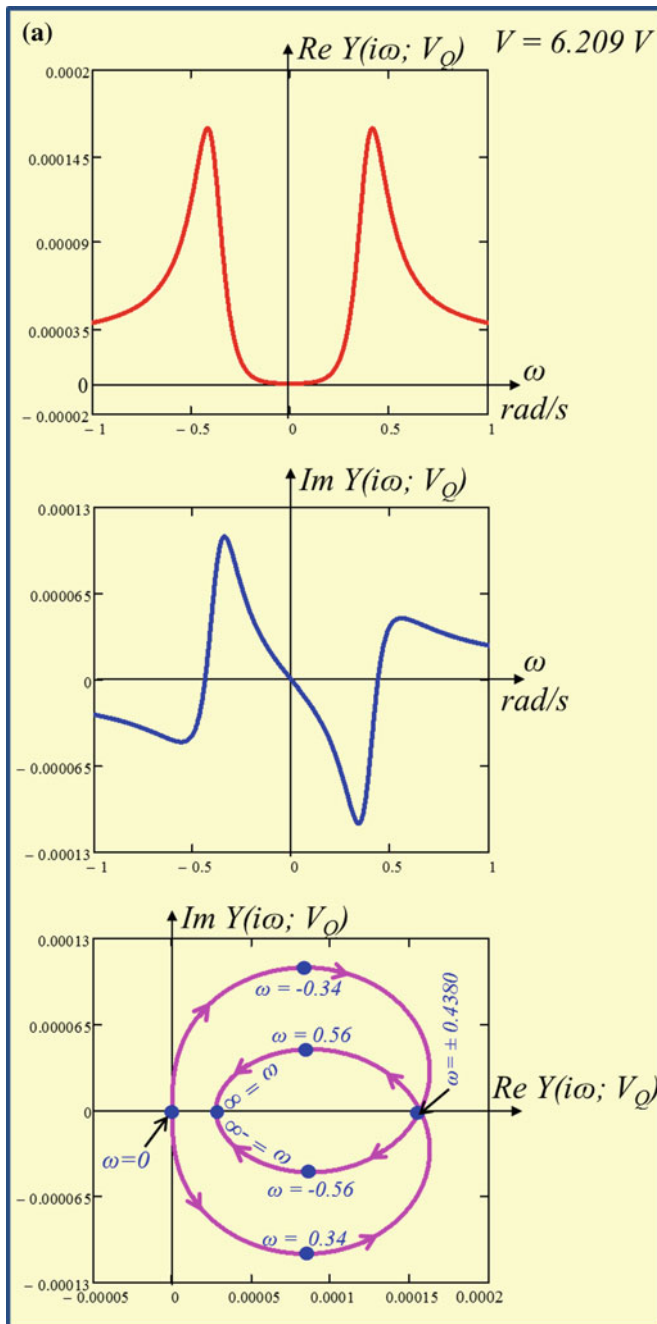


Fig. 10 Small-signal admittance frequency response $\text{Re } Y(i\omega; V_Q)$, $\text{Im } Y(i\omega; V_Q)$ and Nyquist plot of our second-order memristor at **a** $V = 6.209 \text{ V}$, **b** $V = 6.3 \text{ V}$, and **c** $V = 7 \text{ V}$

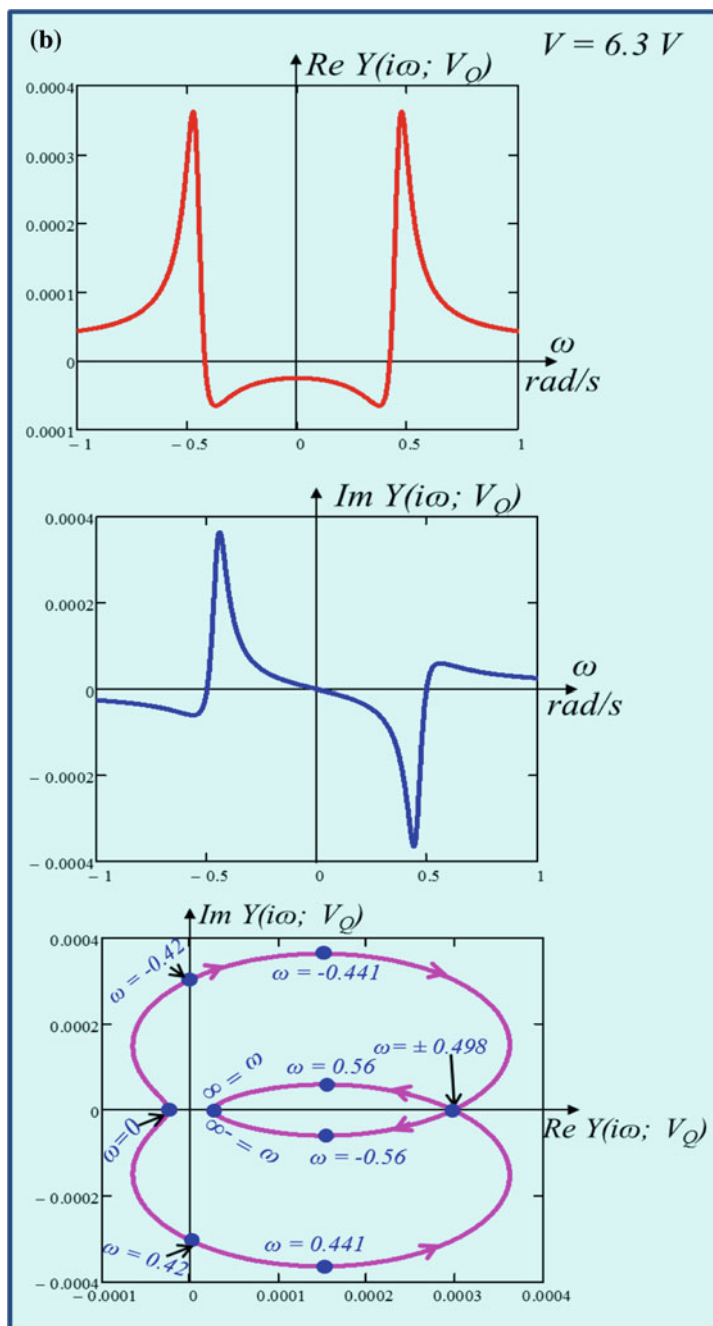


Fig. 10 (continued)

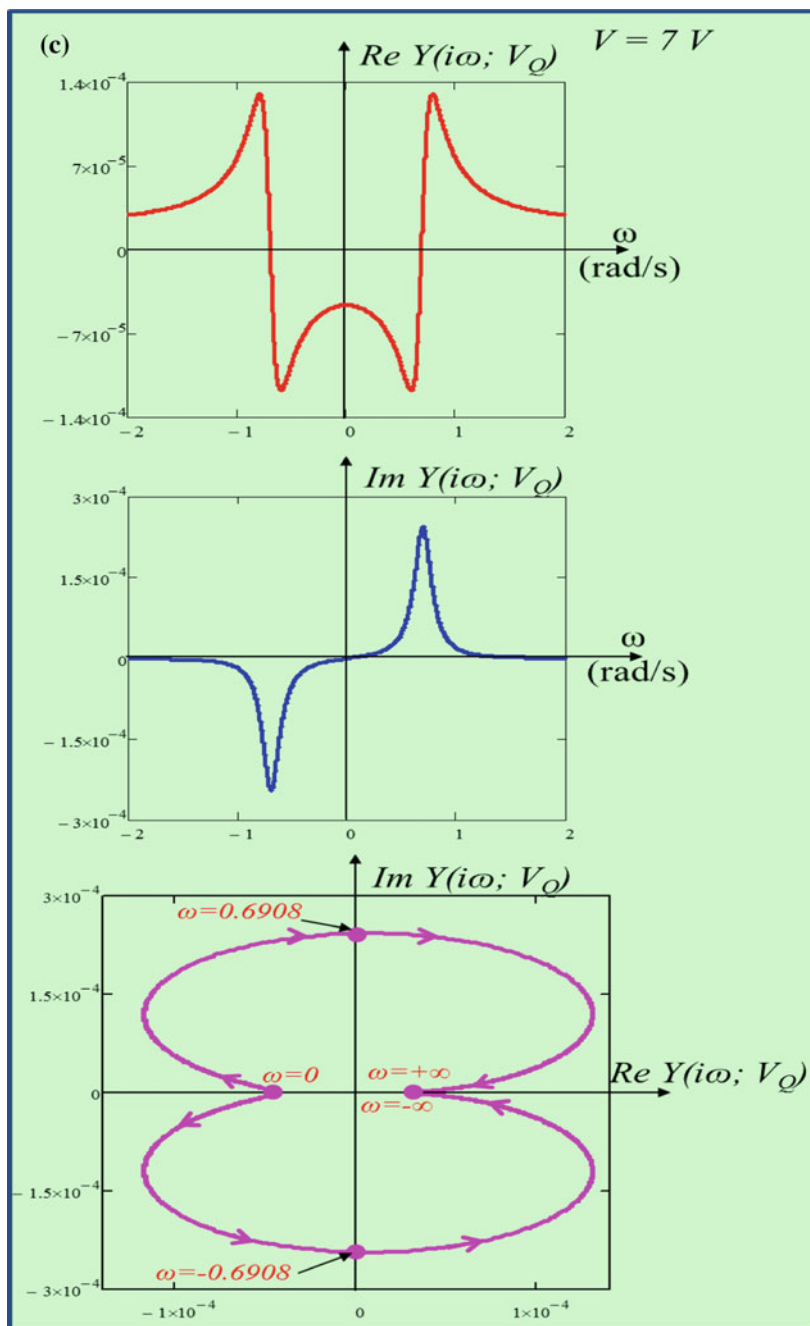


Fig. 10 (continued)

$$\frac{dx_2}{dt} = f_2(x_1, x_2, V) \quad (46b)$$

The Eigen values of the second-order memristor are computed from the Jacobian matrix at the DC equilibrium voltage V obtained by setting the differential Eqs. (46a) and (46b) to zero. Setting $\frac{dx_1}{dt} = 0$ and $\frac{dx_2}{dt} = 0$, and solving for $x_1 = X_1(V)$, $x_2 = X_2(V)$ at V , we obtain the following Jacobian matrix at $(X_1(V), X_2(V))$:

$$J(X_1, X_2; V) = \begin{bmatrix} \frac{\partial f_1(x_1, x_2; V)}{\partial x_1} & \frac{\partial f_1(x_1, x_2; V)}{\partial x_2} \\ \frac{\partial f_2(x_1, x_2; V)}{\partial x_1} & \frac{\partial f_2(x_1, x_2; V)}{\partial x_2} \end{bmatrix}_{(x_1 = X_1(V), x_2 = X_2(V))} \quad (47)$$

According to the theory developed by Chua et al. (1987, 2012a, b) the Eigen values of the Jacobian matrix are identical to the poles³ of the admittance functions $Y(s; V)$. Table 4 illustrates the Eigen values computed from Jacobian matrix (47) and the poles computed from the denominator of the admittance function $Y(s; V)$ in (43). Observe from the Table 4 that the locations of the poles obtained from the admittance function of the second order memristor in Fig. 1c are identical to the Eigen values computed from the Jacobian matrix evaluated at V . Similarly, Fig. 11a and b show plots of the loci of poles of the admittance function $Y(s; V)$, and the loci of Eigen values of the Jacobian matrix as a function of DC equilibrium voltage V in the interval of $-20 \text{ V} \leq V \leq 20 \text{ V}$ whereas to avoid clutter, the arrowheads indicate the movements of poles and the Eigen values only in the interval of $-20 \text{ V} \leq V \leq 0 \text{ V}$. Our numerical simulations show identical results from these two independent methods, as expected. In both the plots of Fig. 11a and b, as the voltage increases the poles of admittance function and the Eigen values also increases. For $V = 0 \text{ V}$, the value of p_1 and p_2 is -0.5 and -1 , respectively, in the pole diagram of admittance function as well as in the Eigen values of the Jacobian matrix whereas $V \leq 6.03481 \text{ V}$ and $V \geq 11.1305 \text{ V}$ the $\text{Im } p_1$ and $\text{Im } p_2$ become zero.

³We would like to caution the readers that the DC current I_{ext} is the *input* in Chua et al. (2012a, b), and the two small-signal equivalent circuits of the potassium ion-channel memristor and the sodium ion-channel memristor in the HH model are connected parallel. Hence, the Eigen values of the Jacobian matrix are identical to the *poles* of the small-signal impedance $Z(s, I) \triangleq \frac{V(s)}{I(s)} = \frac{1}{Y(s)}$, or equivalently, the *zeros* of the admittance $Y(s)$. In the 2nd-order memristor case, the *input* is a DC voltage V and the two small-signal circuit components shown in Fig. 8 are connected in series. It follows that the *poles* of the admittance function $Y(s, V) \triangleq \frac{I(s)}{V(s)}$ of the second-order memristor in Fig. 1c are equivalent to the *Eigen values* of the Jacobian matrix (47).

Table 4 Comparison of the *poles* of the admittance function $Y(s; V)$ and the *Eigen values* of the Jacobian matrix $J(X_1, X_2; V)$

| V | Poles of the admittance function $Y(s; V)$ | Eigen values of the Jacobian Matrix $J(X_1, X_2; V)$ |
|---------------|--|--|
| 0 | -0.5, -1 | -0.5, -1 |
| 1 | -0.4946059, -0.9987707 | -0.4946059, -0.9987707 |
| 2 | -0.4777081, -0.9947101 | -0.4777081, -0.9947101 |
| 3 | -0.4467612, -0.9863768 | -0.4467612, -0.9863768 |
| 4 | -0.3955726, -0.9695863 | -0.3955726, -0.9695863 |
| 5 | -0.3066828, -0.9280549 | -0.3066828, -0.9280549 |
| 6 | -0.1341699, -0.4813821 | -0.1341699, -0.4813821 |
| 6.38820157073 | $\pm 0.50372249 i$ | $\pm 0.50372249 i$ |
| 7 | $0.0958965 \pm 0.6948223 i$ | $0.0958965 \pm 0.6948223 i$ |
| 7.66131678261 | $\pm 0.82930627 i$ | $\pm 0.82930627 i$ |
| 8 | $-0.0995709 \pm 0.8814635 i$ | $-0.0995709 \pm 0.8814635 i$ |
| 9 | $-0.4856009 \pm 0.9272146 i$ | $-0.4856009 \pm 0.9272146 i$ |
| 10 | $-0.8945248 \pm 0.7769816 i$ | $-0.8945248 \pm 0.7769816 i$ |

5 Local Activity and Edge of Chaos

The *local activity theorem* provides the fundamental concept for predicting whether the nonlinear system can exhibit complexity or not, whereas a small neighborhood of the *edge of chaos* in the parameter space of a dynamical system is where *complex phenomena and information processing* will most likely emerge (Chua et al. 1987; Chua 1998; Dogaru and Chua 1998; Vaidyanathan and Volos 2016a, b). Applying

the above theorem in this paper for the second-order memristor, we found from Figs. 10a and 5d that the memristor is locally active only when $V > 6.209$ V, i.e.

$$\operatorname{Re} Y(i\omega; V_Q) < 0, \text{ for } V > 6.209 \text{ V} \quad (48)$$

Observe from Figs. 9b and 11a that the real part of the poles of $Y(s; V_Q)$ vanishes at $V = 6.38820157073$ V, i.e. the poles of the admittance functions $Y(s; V)$ has a pair of complex poles $p_1 = i0.50372249$ and $p_2 = -i0.50372249$ located on the imaginary axis ($\operatorname{Re} p_i = 0$) at the above applied DC voltage. It follows that the corresponding equilibrium $(X_1(V), X_2(V))$ point is no longer *asymptotically stable*

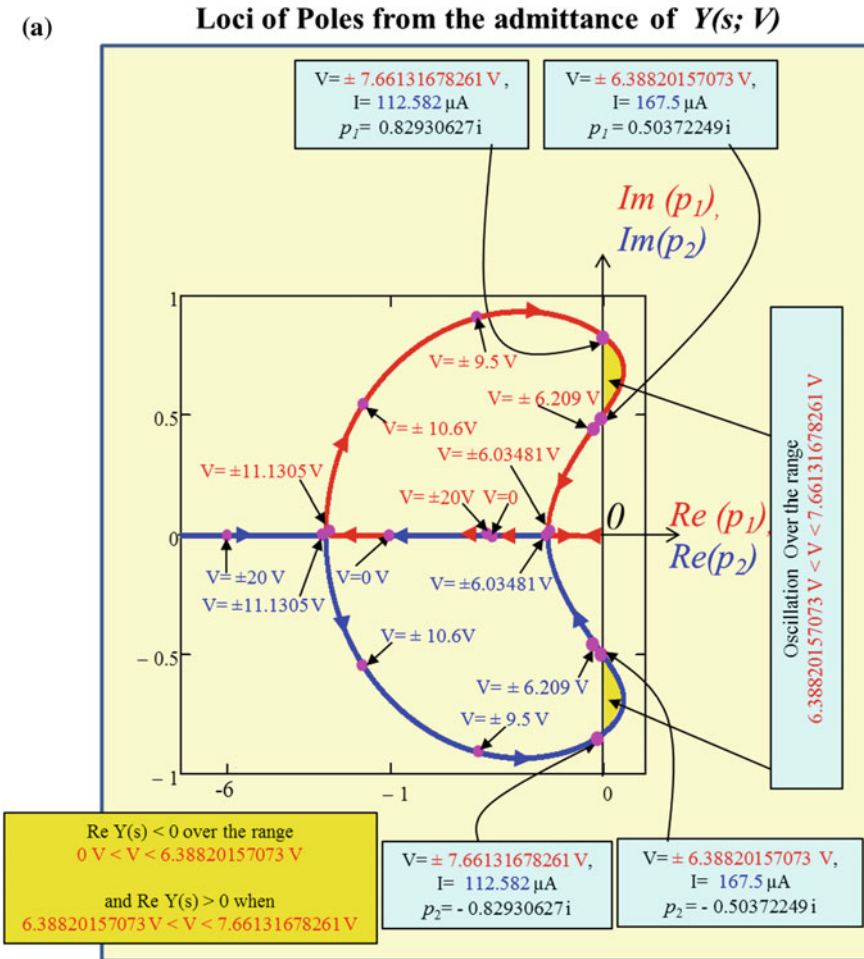


Fig. 11 a Loci of the Poles from the admittance function $Y(s; V)$. b Loci of the Eigen values from the Jacobian matrix $J(X_1, X_2; V)$. Arrowheads indicate the movements of poles and the Eigen values in the interval of $-20 \text{ V} \leq V \leq 0 \text{ V}$

(b)

Loci of Eigen values from the Jacobian Matrix $J(X_1, X_2; V)$

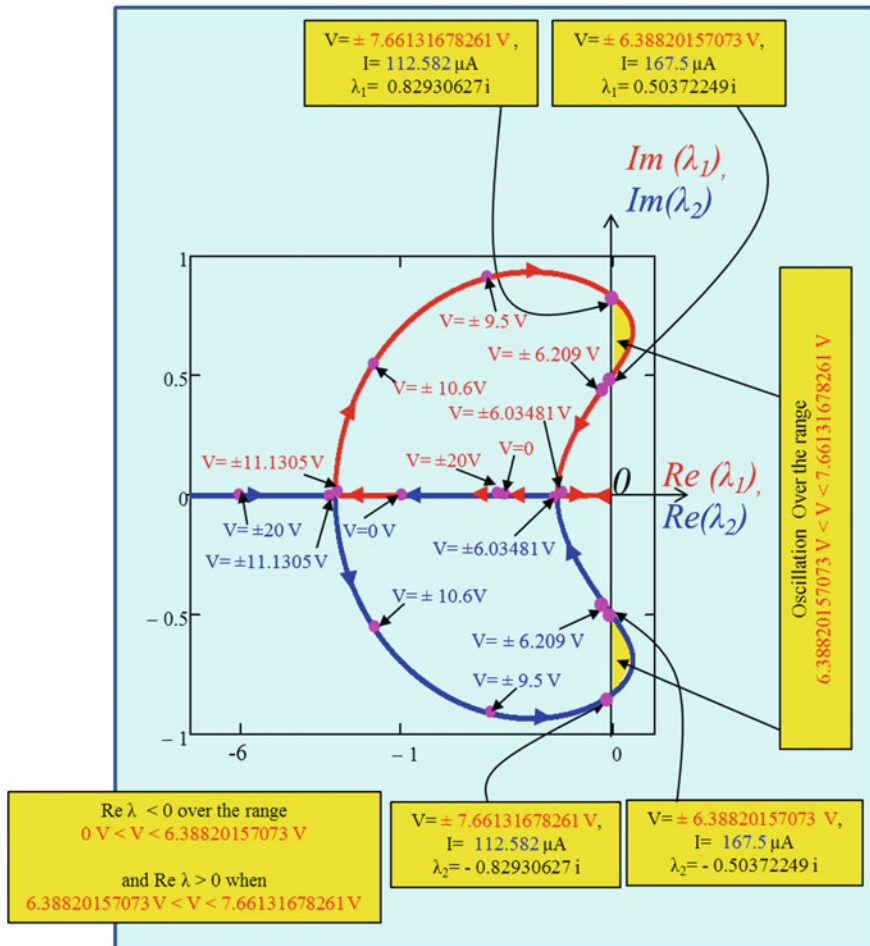


Fig. 11 (continued)

at the above parameter value of V , and becomes unstable thereafter. In other words, the *edge of chaos* regime which started at $V = 6.209 \text{ V}$ (resp. $I = 171.553 \mu\text{A}$) exists only over the following the tiny interval (see Fig. 5d):

Edge of chaos domain 1:
 $6.209 \text{ V} < V < 6.38820157073 \text{ V}$
 $171.553 \mu\text{A} > I > 167.5 \mu\text{A}$

(49)

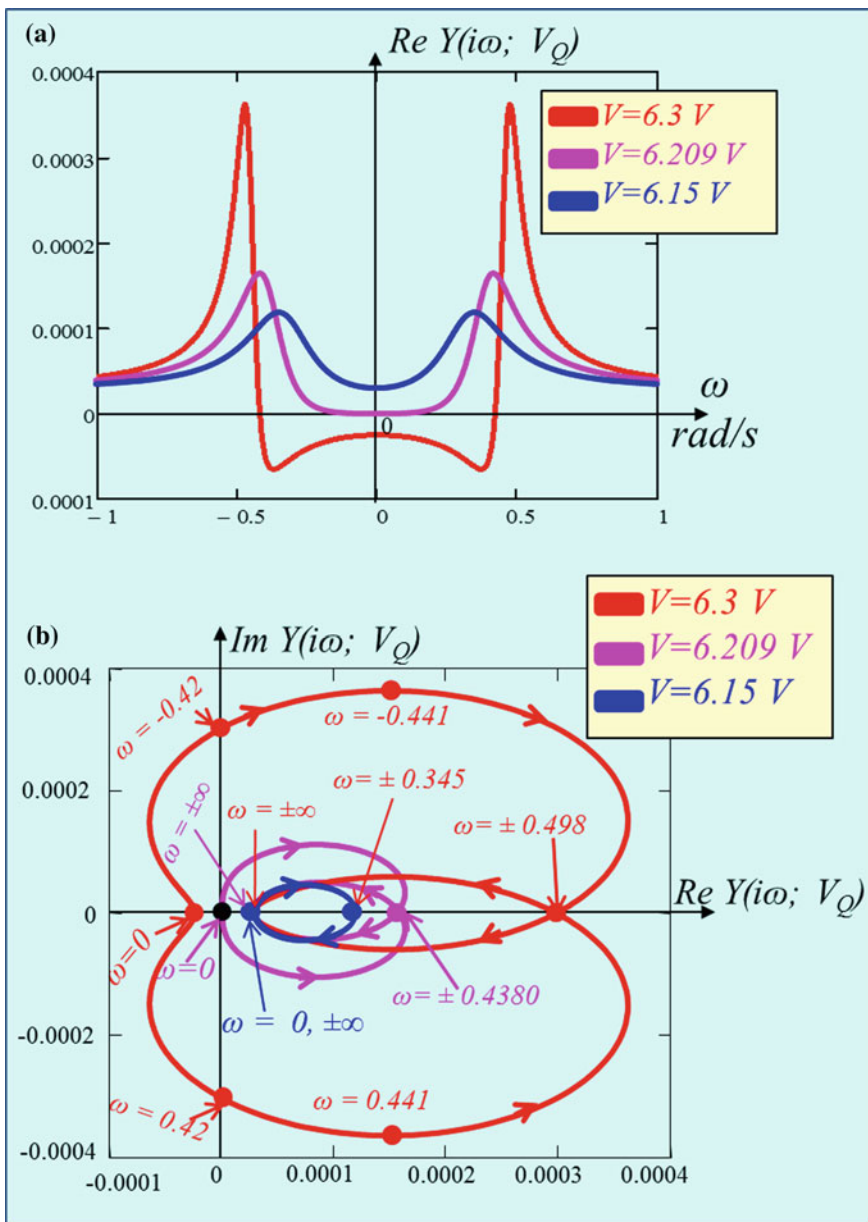


Fig. 12 **a** Illustration of the *principle of local activity* in the second-order memristor at DC input voltage $V = 6.15$ V, $V = 6.209$ V and $V = 6.3$ V. **b** The corresponding Nyquist plot for the input DC voltage $V = 6.15$ V, $V = 6.209$ V and $V = 6.3$ V. **c** Edge of chaos domain 1 and edge of chaos domain 2 on the zoom DC V - I curve of our second-order memristor

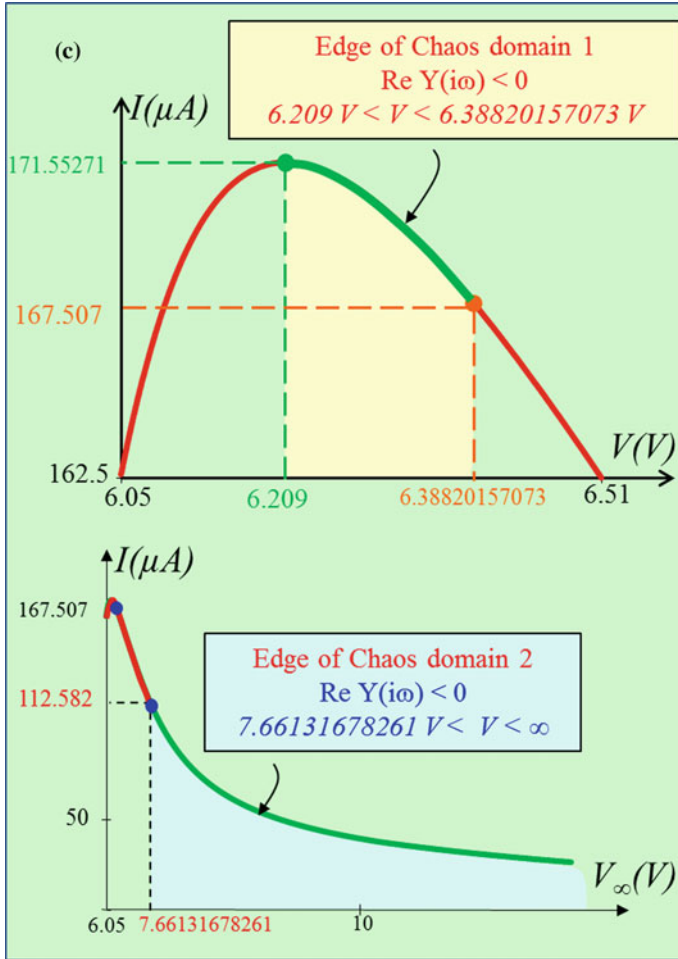


Fig. 12 (continued)

The loci of the two complex poles p_1 and p_2 of $Y(s; V)$ in Fig. 11a reveals the pole p_1 migrated along the red curve in the *right-half plane* to the *left-half plane* as V increases beyond $V = 6.38820157073 \text{ V}$ and crosses the imaginary axis at $V = 7.66131678261 \text{ V}$ (*resp.* $I = 112.582 \mu\text{A}$) where the real part of the pole of $Y(s; V_Q)$ vanishes at $p_1 = -i0.82930627$. Any further increase in the voltage V moves the pole p_1 back into the *left-half plane*. This confirms the existence of a second *edge of chaos* regime starting from $V = 7.66131678261 \text{ V}$ (*resp.* $112.582 \mu\text{A}$), and which extend, over all $V > 7.6613 \text{ V}$ (see Fig. 5d); namely,

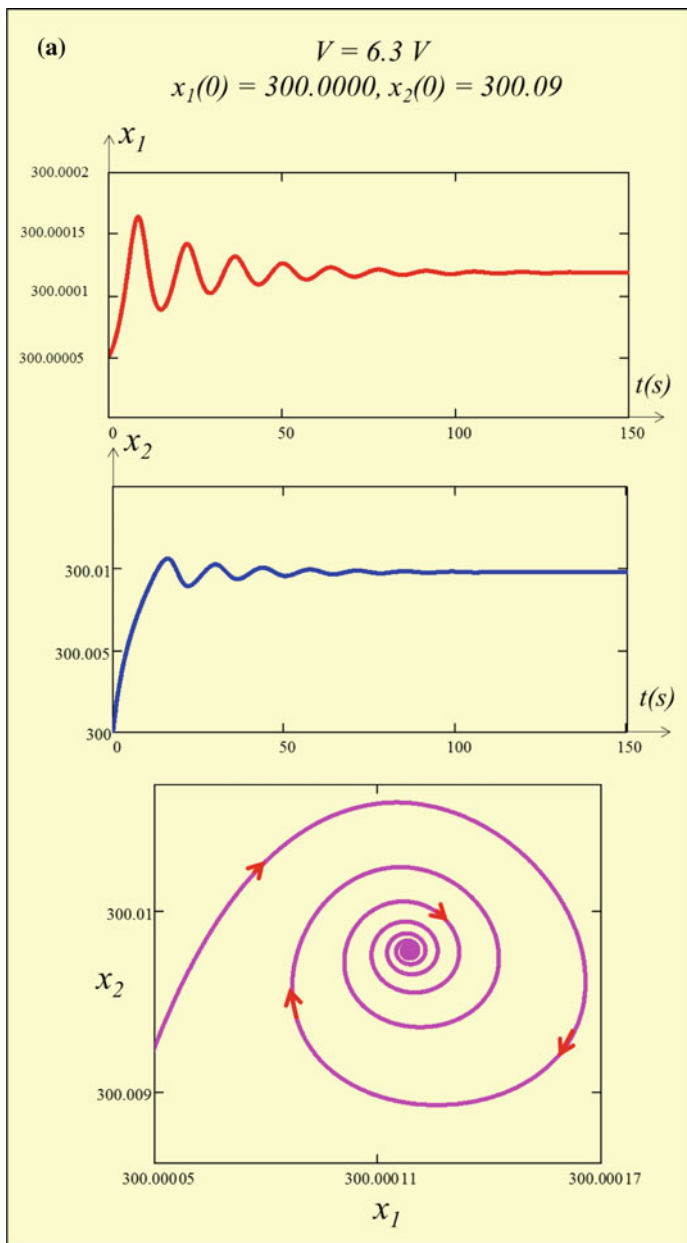


Fig. 13 Numerical Simulations to confirm *super-critical Hopf-bifurcation* theorem at the *first Hopf-bifurcation* $V = 6.38820157073 \text{ V}$ and at the *second Hopf-bifurcation* $V = 7.66131678261 \text{ V}$. **a** Transient waveform converging to DC equilibrium point when the DC voltage $V = 6.3 \text{ V}$ was chosen near but just to the *left* of the *first Hopf-bifurcation* **(b)**. Transient waveform converging to stable oscillation, when $V = 6.4 \text{ V}$ was chosen within the *Hopf super-critical region*. **c** Transient waveform converging to DC equilibrium point when the DC voltage $V = 7.7 \text{ V}$ was chosen near but just to the *left* of the *second Hopf-bifurcation* (see Fig. 11b)

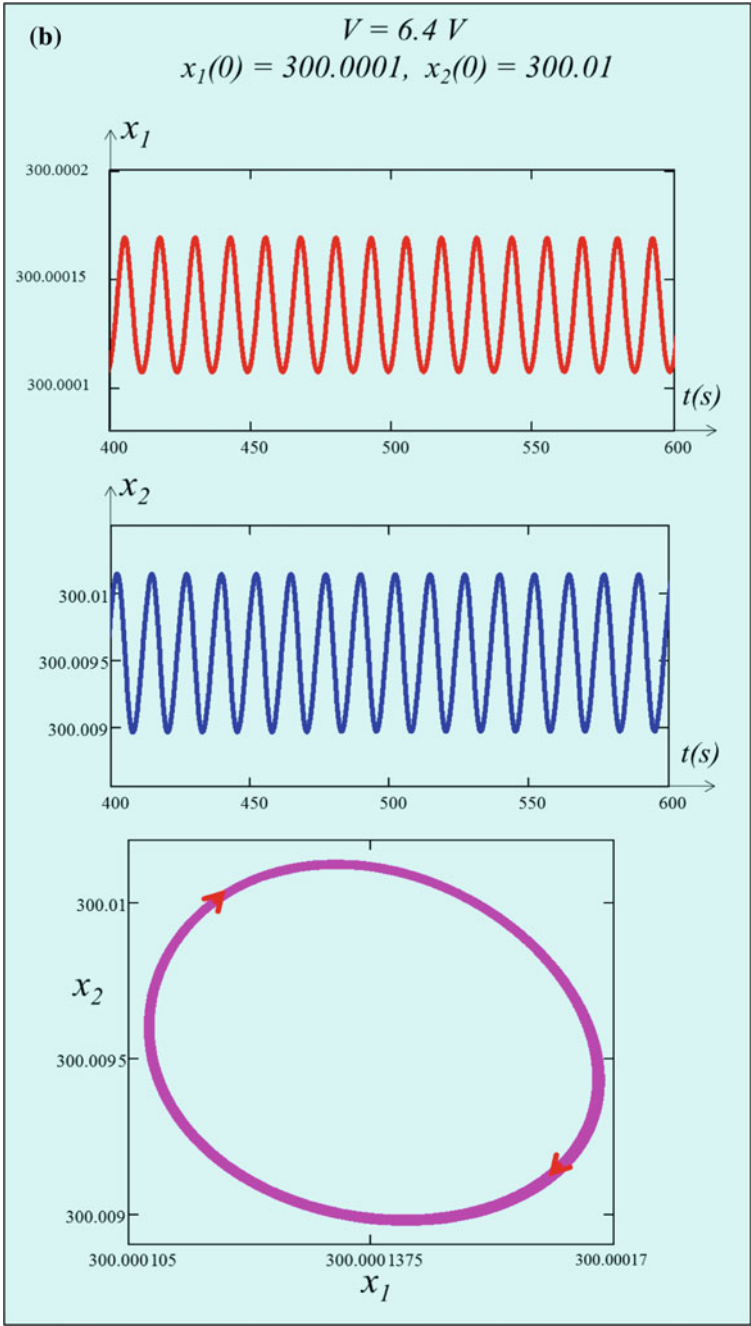


Fig. 13 (continued)

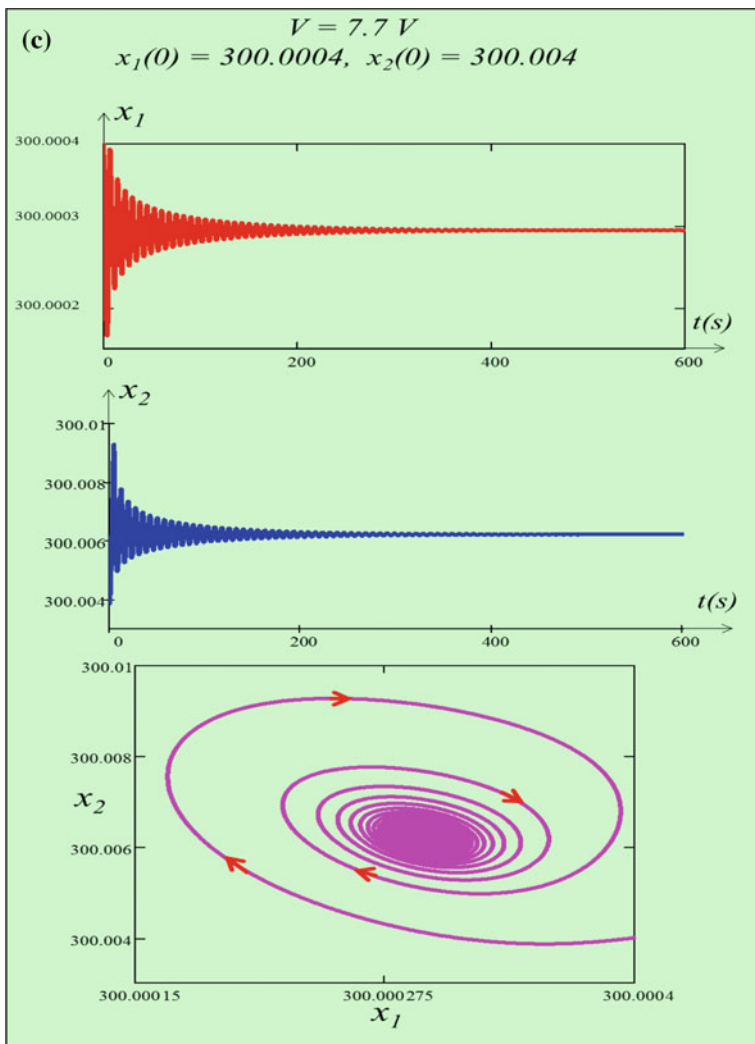


Fig. 13 (continued)

$$\begin{aligned} &\text{Edge of chaos domain 2:} \\ &7.66131678261 \text{ V} < V < \infty \\ &112.582 \mu\text{A} > I > 0 \end{aligned}$$

(50)

To illustrate that *local activity* in the second-order generic memristor starts from $V = 6.209 \text{ V}$, Fig. 12a and b show the plot of $\text{Re}Y(i\omega; V_Q)$ and the corresponding Nyquist plot for the DC input voltage $V = 6.15 \text{ V}$, $V = 6.209 \text{ V}$ and $V = 6.3 \text{ V}$,

respectively. Observe, the Nyquist plot of the admittance function $Y(i\omega; V_Q)$ is tangent to the ω axis at $\omega=0$ for $V = 6.209$ V. Also, observe that for $V = 6.15$ V, the real part of the Nyquist plot of the admittance function is positive, i.e., $\text{Re}Y(i\omega; V_Q) > 0$, confirming the memristor is *not locally active*. However, for $V = 6.3$ V, the real part of the Nyquist plot of the admittance function $Y(i\omega; V_Q)$ is negative confirming that the memristor is *locally active*. The corresponding Nyquist plots in $\text{Im}Y(i\omega; V_Q)$ versus $\text{Re}Y(i\omega; V_Q)$ plane is shown in Fig. 12b. Figure 12c shows the *edge of chaos domain 1* and *edge of chaos domain 2* on the zoom DC V - I curve of our second-order memristor. Observe that in both *edge of chaos domain 1* (49), and *domain 2* (50), we have $\text{Re}Y(i\omega; V_Q) < 0$, $\text{Rep}_1 < 0$, and $\text{Rep}_2 < 0$ (see Figs. 5d and 11a).

6 Hopf Bifurcation

Hopf bifurcation is a local bifurcation generated by non-linear dynamical systems in which an equilibrium point changes stability at some critical parameter value μ , under certain conditions. The bifurcation can be *super-critical* or *sub-critical* resulting in a stable or unstable limit cycle respectively, and is confirmed by the computation of a Hopf coefficient “ a ” at the equilibrium point when a pair of *eigen values* of the associated Jacobian matrix are purely imaginary. The standard *Hopf coefficient* “ a ” for a *second-order ODE* is given by:

$$a = \frac{1}{16} [f_{xxx} + f_{xyy} + g_{xxy} + g_{yyy}] + \frac{1}{16\omega_0} [f_{xy}(f_{xx} + f_{yy}) - g_{xy}(g_{xx} + g_{yy}) - f_{xx}g_{xx} + f_{yy}g_{yy}] \quad (51)$$

The plot of $\text{Im}(\lambda)$ versus $\text{Re}(\lambda)$ shown in Fig. 11b shows, the two Hopf-bifurcation points occur at $V = 6.38820157073$ V and $V = 7.66131678261$ V, respectively where the real parts of the Eigen values of Jacobian matrix at these two points are zero (*pure imaginary Eigen values*). The eigen values within these two bifurcation points lie on the right-half plane ($\text{Re}(\lambda) > 0$), confirming the second-order memristor could generate oscillation. To confirm that these two Hopf-bifurcation points are *super-critical*, let us compute the Hopf coefficient “ a ” at $V = 6.38820157073$ V, where the functions f_1 and f_2 in (46a) and (46b) are denoted by f and g , respectively, in (51).

$$\begin{aligned} a &= 1.826 \times 10^3 > 0 \text{ for } V = 6.38820157073 \text{ V and } \omega_0 = 0.50372249 \\ a &= 1.59 \times 10^3 > 0 \text{ for } V = 6.38820157073 \text{ V and } \omega_0 = -0.50372249 \end{aligned} \quad (52)$$

The coefficient $a > 0$ at the first Hopf-bifurcation point ($V = 6.38820157073 \text{ V}$) implies the bifurcation is *super-critical* because the parameter $\mu = V$ enters the *unstable region* ($\text{Re}(\lambda) > 0$) by crossing the imaginary axis from *left to right* in Fig. 11a. Similarly, the Hopf coefficient “ a ” at the second Hopf-bifurcation point at $V = 7.66131678261 \text{ V}$ is found to be

$$\begin{aligned} a &= -1.155 \times 10^3 < 0 \text{ for } V = 7.66131678261 \text{ and } \omega_0 = 0.82930627 \\ a &= -1.239 \times 10^3 < 0 \text{ for } V = 7.66131678261 \text{ and } \omega_0 = -0.82930627 \end{aligned} \quad (53)$$

The coefficient $a < 0$ at the second Hopf-Bifurcation point ($V = 7.66131678261 \text{ V}$) actually implies the bifurcation is *super-critical* because the parameter $\mu = V$ returns to the *stable region* ($\text{Re}(\lambda) < 0$) by crossing the imaginary axis from *right to left*, as the parameter $\mu = V$ increases beyond the bifurcation value $V = 7.66131678261 \text{ V}$. The formula given in all standard

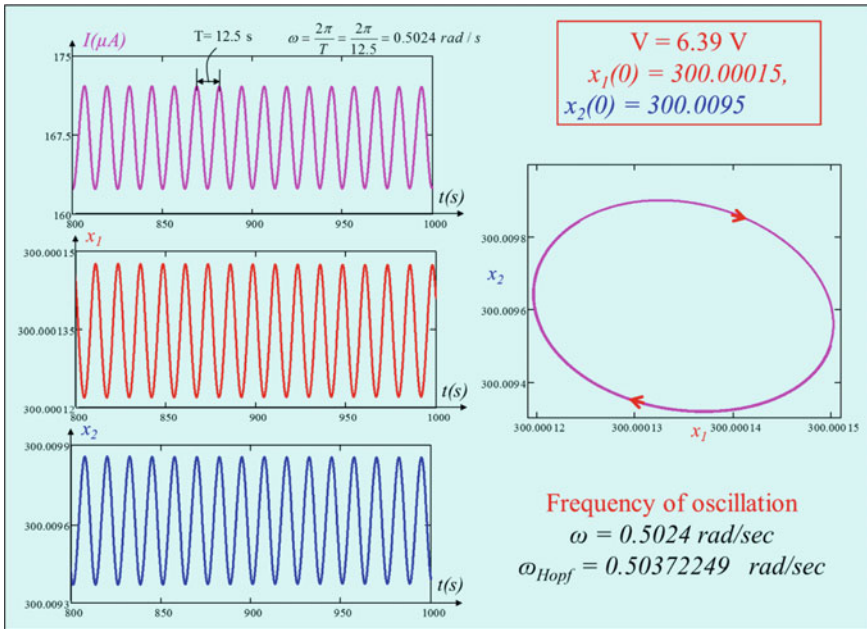


Fig. 14 An example illustrating the frequency of oscillation ω is very close to the predicted Hopf frequency ω_{Hopf} at $V = 6.39 \text{ V}$

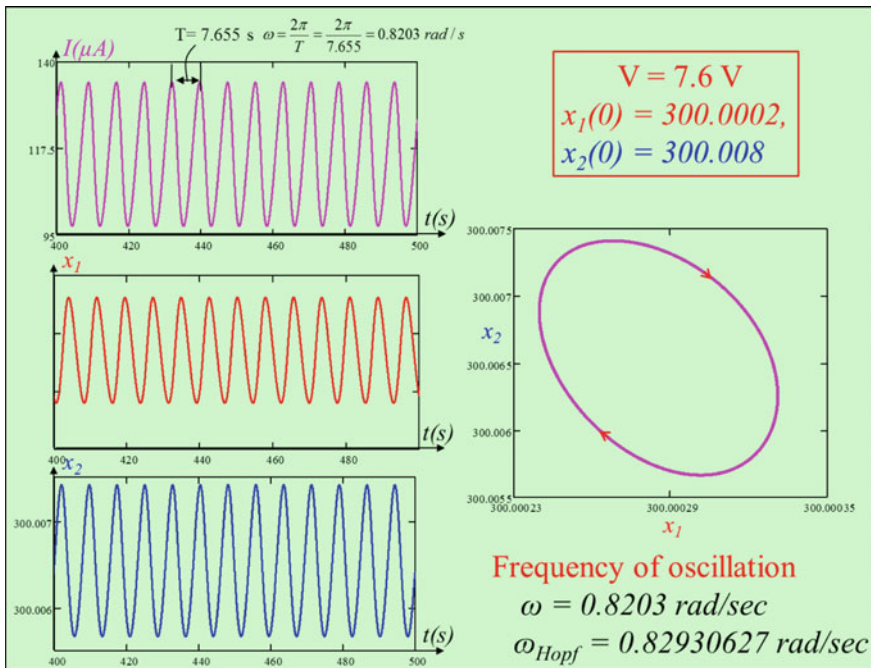


Fig. 15 An example illustrating the frequency of oscillation ω is very close to the predicted Hopf frequency ω_{Hopf} at $V = 7.6$ V

textbooks (Meiss 2007) for the Hopf coefficient “ a ” was derived by *assuming* the system becomes unstable ($\text{Re}(\lambda) > 0$) as the parameter μ crosses the imaginary axis from *left to right*, as μ *increases* beyond the Hopf-bifurcation point. It follows from the *super-critical Hopf-bifurcation theorem* that there exists a small sinusoidal oscillation for any value of the DC voltage V chosen sufficiently near but greater than the right boundary at $V = 6.38820157073$ V, and the right boundary at $V = 7.66131678261$ V where the equilibrium point is unstable. However, any initial state beyond *super-critical region* converges to another *stable equilibrium* point. We verified this phenomenon in our second-order memristor by choosing voltage $V = 6.3$ V, which is near but slightly to the left of the *first Hopf-bifurcation* point at $V = 6.38820157073$ V. Observe from Fig. 13a that the transient waveform converges to an asymptotically *stable equilibrium* point. An *identical* phenomenon was observed as shown in Fig. 13c, where the DC input voltage $V = 7.7$ V was chosen near but to the left of the *second Hopf bifurcation* point at $V = 7.66131678261$ V. However, the transient waveform converges to a *stable limit cycle* as shown in Fig. 13b, when $V = 6.4$ V was chosen within the *Hopf super-critical region*.

Numerical simulations are performed within the super-critical Hopf region near the two bifurcation points to confirm that the frequency of the oscillation is close to

the predicted Hopf frequency. Figures 14 and 15 show examples of the waveforms obtained at $V = 6.39$ V (near but to the right of the first Hopf-bifurcation point $V = 6.38820157073$ V, see Fig. 11b) and at $V = 7.6$ V (near and to the right of the second Hopf bifurcation point $V = 7.66131678261$ V, see Fig. 11b). Observe that the waveforms corresponding to $V = 6.39$ V and $V = 7.6$ V converged to a stable limit cycle with frequency $\omega = 0.5024$ rad/s, and $\omega = 0.8203$ rad/s, respectively, which are very close to the predicted Hopf frequency $\omega = 0.50372249$ rad/s, and $\omega = 0.82930627$ rad/s, respectively.

7 Concluding Remarks

This paper presented a simple electronic oscillator using a second-order memristor (Chua 2014), and a battery. According to Chua (1969), the simplest mathematical oscillator circuit must contain a second-order autonomous nonlinear differential equation. The simulation results of the two differential equations $x_1(t)$ and $x_2(t)$ showed almost sinusoidal oscillations and the stability of the oscillation is verified via phase analysis. Our simulation results showed the edge of chaos regime *domain 1* and *domain 2* lie between the intervals $6.209 \text{ V} < V < 6.38820157073 \text{ V}$, and $7.66131678261 \text{ V} < V < \infty$, respectively in DC V - I curve, whereas the Hopf super-critical regime lie between the interval $6.38820157073 \text{ V} < V < 7.66131678261 \text{ V}$. Beyond both ends of the super-critical interval, the circuit tends to a DC equilibrium point on the DC V - I curve. A small-signal equivalent circuit was derived by choosing a DC equilibrium point Q and are found to consist of two identical linear resistor-inductor (RL) sub-circuits (with different resistance and inductance values) connected in series. The poles of the admittance function $Y(s; V)$ are shown to be identical to the *Eigen values* of the Jacobian matrix of this small-signal equivalent circuit describing the memristor-battery circuit. At $V = 6.38820157073$ V and at $V = 7.66131678261$ V, the loci of the *Eigen value* as a function of the DC voltage V crosses the imaginary axis. We found, all the initial conditions decay to a DC operating point, if we increase the battery voltage V from $V = 0$ V to the left boundary of the edge of chaos at $V = 6.209$ V. A further increase in V causes the pair of complex-conjugate *Eigen values* to cross the imaginary axis, while spawning a small sinusoidal oscillation whose amplitude increases rapidly (like the square root of 2) with increasing battery voltage. This phenomenon of a super-critical Hopf bifurcation (Meiss 2007) serves as a textbook example, which we had confirmed analytically by showing the Hopf bifurcation coefficient “ a ” is positive. On the other hand, the amplitude of the oscillation begins to decrease, with further increase in battery voltage V , illustrating the prediction of the Hopf bifurcation theorem no longer exists.

Similarly, when the battery voltage is decreased from far beyond the right boundary of the edge of chaos *domain 2* at $V = 7.66131678261$ V, we found once again all initial conditions converge to a DC operating point at the corresponding battery voltage. Furthermore, when the battery voltage reaches the left boundary of

the edge of chaos *domain 2* at $V = 7.66131678261$ V then the pair of complex-conjugate *Eigen values* crosses the imaginary axis from *right to left* while spawning another small sinusoidal oscillation, whose amplitude increases rapidly like before, as we continue to *decrease* the battery voltage. Soon the sinusoidal waveform merges seamlessly with the earlier sinusoidal waveform spawned from the right boundary of the edge of chaos *domain 1*!

Indeed, we have also proved that the second-order memristor oscillator could generate sinusoidal oscillation via a *super-critical* Hopf bifurcation. In this paper, the computation of Hopf bifurcation coefficient “ a ” gives a < 0 in contrast to the standard Hopf bifurcation condition which satisfies that $a > 0$. The reason for the above difference in the sign of “ a ” is due to the fact that the calculation of Hopf bifurcation coefficient “ a ” described in nonlinear dynamics textbooks (Meiss 2007) is based on the assumption that the pair of complex-conjugate *Eigen values* crosses the imaginary axis from *left to right* as the bifurcation parameter *increases*.

Finally, we conclude that the memristor-battery oscillator gives rise to two sinusoidal oscillations originating from either boundary of the edge of chaos regime of the memristor via *super-critical* Hopf bifurcation and it also provides the textbook example for detail understanding of *super-critical* Hopf bifurcation phenomenon.⁴ In this paper, the second order memristor represents the model of a physical device called *Positive Temperature Coefficient (PTC)* and *Negative Temperature Coefficient (NTC)* thermistor connected in series. So, as a future work, it is possible to generate oscillations in a real circuit by connecting *PTC* and *NTC* thermistors in series across the battery via *super-critical* Hopf bifurcation phenomenon.

Acknowledgements The authors would like to acknowledge financial support from the USA Air force office of Scientific Research under Grant number FA9550-13-1-0136 and from the European Commission Marie Curie Fellowship and two National Research Foundation of Korea (NRF) grants funded by the Korea government (2013R1A2A2A01068683 and 2012R1A1A2044078).

References

- Adhikari, S. P., Sah, M. P., Kim, H., & Chua, L. O. (2013). Three fingerprints of memristors. *IEEE Transactions on Circuits and Systems I: Regular Papers*, 60, 3008–3021.
- Chua, L. O. (1969). *Introduction to nonlinear network theory*. New York: McGraw-Hill.
- Chua, L. O., & Kang, S. M. (1976). Memristive devices and systems. *Proceedings of the IEEE*, 64, 209–223.
- Chua, L. O., Desoer, C. A., & Kuh, E. S. (1987). *Linear and nonlinear circuits*. New York: McGraw-Hill.

⁴In contrast, the second-order sodium ion-channel memristor oscillator circuit presented in Fig. 40 of Chua (2014) spawns an *unstable* sinusoidal oscillation near a boundary of the edge of chaos of the sodium memristor via a *sub-critical* Hopf bifurcation, a much more subtle bifurcation phenomenon.

- Chua, L. O. (1998). *CNN: A paradigm for complexity*. Singapore: World Scientific.
- Chua, L. O. (2003). Nonlinear circuit foundations for nanodevices—Part I: The four element torus. *Proceedings of the IEEE*, 91, 1830–1859.
- Chua, L., Sbitnev, V., & Kim, H. (2012a). Hodgkin-Huxley axon is made of memristors. *International Journal of Bifurcation and Chaos*, 22, 1230011/1-48.
- Chua, L., Sbitnev, V., & Kim, H. (2012b). Neurons are poised near the edge of chaos. *International Journal of Bifurcation and Chaos*, 22, 1250098/1-49.
- Chua, L. (2014). If it's pinched it's a memristor. *Semiconductor Science and Technology*, 29, 104001/1-42.
- Chua, L. (2015). Everything you wish to know about memristors but are afraid to ask. *Radio Engineering*, 24, 2/319-368.
- Dogaru, R., & Chua, L. O. (1998). Edge of chaos and local activity domain of FitzHugh-Nagumo equation. *International Journal of Bifurcation and Chaos*, 8, 211–257.
- Mannan, Z. I., Choi, H., & Kim, H. (2016). Chua corsage memristor oscillator via Hopf bifurcation. *International Journal of Bifurcation and Chaos*, 26, 1630009/1–28.
- Mehta, V. K., & Mehta, R. (2005). *Principle of electronics*. India: S. Chand and Co., Ltd.
- Meiss, J. D. (2007). *Differential dynamical systems*. USA: Society of Industrial and Applied Mathematics.
- Rajamani, V., Yang, C., Kim, H., & Chua, L. (2016). Design of a low-frequency oscillator with ptc memristor and an inductor. *International Journal of Bifurcation and Chaos*, 26, 1630021/1-27.
- Vaidyanathan, S., & Volos, C. (2016a). *Advances and applications in nonlinear control systems*. Berlin: Springer.
- Vaidyanathan, S., & Volos, C. (2016b). *Advances and applications in chaotic systems*. Berlin: Springer.

Advances in Memristors, Memristive Devices and
Systems

Vaidyanathan, S.; Volos, C. (Eds.)

2017, XII, 511 p. 294 illus., 229 illus. in color.,

Hardcover

ISBN: 978-3-319-51723-0